

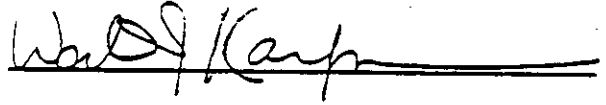
**SELF ADAPTIVE MESH IN STRESS ANALYSIS**

**Paolo Roberti**

**1984**  
**Report No. CSD-840032**

**MASTER COPY**

The dissertation of Paolo Francesco G. Roberti is approved.



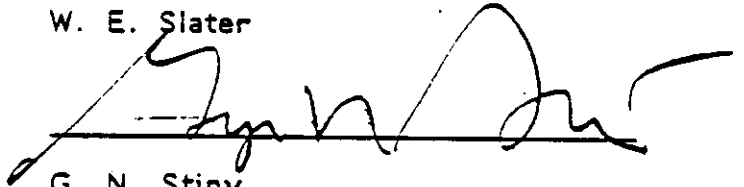
W. J. Karplus



R. D. Nelson



W. E. Slater



G. N. Stiny



M. A. Melkanoff, Committee Chair

University of California, Los Angeles

1984

## CONTENTS

LIST OF SYMBOLS . . . . .	v
ACKNOWLEDGEMENTS . . . . .	xi
VITA . . . . .	xii
PUBLICATIONS . . . . .	xii
ABSTRACT OF THE DISSERTATION . . . . .	xiii

<u>Chapter</u>	<u>page</u>
I. INTRODUCTION . . . . .	1
II. THE BLACK BOX APPROACH . . . . .	3
III. SELF-ADAPTIVE ANALYSIS PACKAGES . . . . .	6
IV. A NEW EXPERIMENTAL SELF-ADAPTIVE SYSTEM . . . . .	11
V. INTERNAL ORGANIZATION OF THE NEW SYSTEM . . . . .	13
Elements used . . . . .	13
Initial meshing . . . . .	14
Enrichment algorithm . . . . .	14
Criteria used for the error indicator . . . . .	34
Criteria used for truss bars . . . . .	34
Criteria used for triangles . . . . .	34
Overall system organization . . . . .	36
VI. ERROR ESTIMATE OF STRESSES . . . . .	39
Error Estimate of axial stress in truss bars . . . . .	39
Error estimate of stresses in triangles . . . . .	42
Basic assumptions . . . . .	42
The error stress tensor . . . . .	44
Error estimate . . . . .	45
Precision of Error Estimate of stresses . . . . .	47
False convergence . . . . .	50
Treatment of singularities . . . . .	52

VII.	COMPUTER IMPLEMENTATION AND EXAMPLES . . . . .	53
	Computer implementation . . . . .	53
	Example no. 1 . . . . .	54
	Example no. 2 . . . . .	67
	Example no. 3 . . . . .	74
	Example no. 4 . . . . .	91
VIII.	EXTENSION OF THE PRESENT SYSTEM TO ANALYZE SHELL STRUCTURES . . . . .	104
IX.	CONCLUSIONS . . . . .	106
	<u>Appendix</u> . . . . .	<u>page</u>
A.	PRECISION OF ERROR ESTIMATE IN ONE DIMENSION . . . . .	108
	REFERENCES . . . . .	111

## LIST OF SYMBOLS

- $\sigma_{ij}^*$  = exact stress tensor
- $\sigma_{ij}$  = approximate stress tensor calculated during the last analysis
- $\tau_{ij}$  = approximate stress tensor calculated during the analysis preceding the last one
- $\delta_{ij}$  = difference stress tensor
- $\|\delta_{ij}\|$  = norm of the difference stress tensor
- $\|\delta_{ij}\|_m$  = maximum value of the norms of the difference stress tensor in the three adjacent triangles
- $\varepsilon_{ij}$  = error stress tensor
- $\|\varepsilon_{ij}\|$  = norm of the error stress tensor
- $r$  = ratio between true error and error estimate
- $x$  = independent variable in the Poisson problem in one dimension
- $l$  = upper limit to the domain of  $x$
- $u$  = solution of Poisson problem in one dimension
- $f(x)$  = right hand side of the Poisson problem in one dimension
- $a_n$  = constants in the Taylor series expansion
- $n$  = degree of the first non zero polynomial in the Taylor expansion

$d_i$  = element size in one dimension

$s_i$  = FEM approximation of the derivatives in one dimension

$D_i$  = error indicator in one dimension

$E_i$  = true error in one dimension

## LIST OF TABLES

<u>Table</u>	<u>page</u>
1. Example of Error Underestimation (1-D) . . . . .	49
2. Highest Error Stress Tensor Norms, Example no. 1 . . . . .	61
3. Corners Coordinates . . . . .	65
4. Stresses at Corner, Case 1 . . . . .	65
5. Stresses at Corner, Case 2 . . . . .	65
6. Corners Coordinates . . . . .	66
7. Stresses at Corner, Case 1 . . . . .	66
8. Stresses at Corner, Case 2 . . . . .	67
9. Highest Error Stress Tensor Norms, Example no. 2 . . . . .	75
10. Stresses at Corner, Case 1 . . . . .	88
11. Stresses at Corner, Case 2 . . . . .	88
12. Stresses at the Centroid, Case 1 . . . . .	89
13. Stresses at the Centroid, Case 2 . . . . .	89
14. Taylor Series Expansion, Case 1 . . . . .	90
15. Taylor Series Expansion, case 2 . . . . .	91
16. Highest Error Stress Tensor Norms, Example no. 3 . . . . .	102
17. Highest Error of Axial Stress in Truss Bars, Example no. 3 . . . . .	102

## LIST OF FIGURES

<u>Figure</u>	<u>page</u>
1. Triangles marked to be split . . . . .	17
2. Triangles after splitting in step 1 . . . . .	18
3. Triangles marked to be split in step 2 . . . . .	19
4. Triangles after splitting in step 2 . . . . .	20
5. Triangles marked to be split in step 3 . . . . .	21
6. Triangles after splitting in step 3 . . . . .	22
7. Triangles marked to be split in step 4 (first pass) . . . . .	23
8. Triangles after splitting in step 5 (first pass) . . . . .	24
9. Triangles marked to be split in step 4 (second pass) . . . . .	25
10. Triangles after splitting in step 5 (second pass) . . . . .	26
11. Triangles marked to be split in step 4 (third pass) . . . . .	27
12. Triangles after splitting in step 5 (third pass) . . . . .	28
13. Non-conforming edge facing more than two triangles (frame1)	30
14. Non-conforming edge facing more than two triangles (frame2)	31
15. Non-conforming edge facing more than two triangles (frame3)	32
16. System flowchart . . . . .	38
17. Error estimate in truss bars . . . . .	41
18. Error estimate in triangles . . . . .	43
19. Case of false convergence . . . . .	52
20. Example no. 1, description of the problem . . . . .	56



21.	Example no. 1, input to the system . . . . .	57
22.	Example no. 1, mesh at iteration 1 . . . . .	58
23.	Example no. 1, mesh at iteration 7 . . . . .	59
24.	Example no. 1, color coded stress levels . . . . .	60
25.	Example no. 1, initial mesh, second run . . . . .	63
26.	Example no. 1, final mesh, second run . . . . .	64
27.	Example no. 2, description of the problem . . . . .	69
28.	Example no. 2, input to the system . . . . .	70
29.	Example no. 2, mesh at iteration 1 . . . . .	71
30.	Example no. 2, mesh at iteration 7 . . . . .	72
31.	Example no. 2, color coded stress levels . . . . .	74
32.	Example no. 3, description of the problem . . . . .	76
33.	Example no. 3, input to the system . . . . .	77
34.	Example no. 3, initial mesh . . . . .	78
35.	Example no. 3, mesh at iteration 8 . . . . .	80
36.	Example no. 3, non-converged area at iteration 8 . . . . .	81
37.	Example no. 3, mesh at iteration 9 . . . . .	82
38.	Example no. 3, non-converged area at iteration 9 . . . . .	83
39.	Example no. 3, color coded stress levels at iteration 9 . . . . .	84
40.	Triangle with error stress tensor norm larger than 5 ksi, case 1 . . . . .	86
41.	Triangle with error stress tensor norm larger than 5 ksi, case 2 . . . . .	87
42.	Example no. 3, description of the problem . . . . .	93
43.	Example no. 3, input to the system . . . . .	94
44.	Example no. 3, mesh at iteration 1 . . . . .	95
45.	Example no. 3, mesh at iteration 5 . . . . .	96

46.	Example no. 3, color coded stress levels in the flange s . . . . .	97
47.	Example no. 3, color coded stress levels in the web . . . . .	98
48.	Example no. 3, initial mesh, second run . . . . .	100
49.	Example no. 3, final mesh second run . . . . .	101

## ACKNOWLEDGEMENTS

I would like to thank professor M. A. Melkanoff and professor R. D. Nelson for their support and technical advice. I would also like to thank Jonathan Hart for his collaboration and Miss Fariba Zargarpour for her very helpfull suggestion while reviewing the manuscript.

## VITA

June 18, 1954--Born, Somma Lombardo, Italy

1980--B.S., University of California at Los Angeles

1980--M.S., University of California at Los Angeles

1983--Engineer, University of California at Los Angeles

## PUBLICATIONS

"The Accelerated Power Method", International Journal for Numerical Methods in Engineering, accepted for publication.

ABSTRACT OF THE DISSERTATION

Self Adaptive Mesh in Stress Analysis

by

Paolo Francesco G. Roberti

Doctor of Philosophy in Engineering

University of California, Los Angeles, 1984

Professor M. A. Melkanoff, Chair

A new, design-oriented, approach to stress analysis is presented. This approach is based on the Finite Element Method combined with self-adaptive mesh techniques. It allows the designer to perform stress analysis without outside help and/or any previous knowledge of numerical methods. A 2-D software system has been developed based on this approach. Some examples are given to demonstrate the capabilities of the system. The extension of the system, to perform static analysis of shells in 3-D, is discussed in some detail.



## Chapter I

### INTRODUCTION

The Finite Element Method is not widely used in the design of structural elements, even though the new interactive systems (CAEDS, PATRAN-G) developed recently, have greatly simplified the use of FEM.

The major reason is that FEM, as used today, requires a specialist, called analyst. The analyst is required to work side by side with the designer who is normally not trained in numerical methods. This situation is expensive and time consuming. Whenever the designer and the analyst try to communicate there is a high probability of misunderstanding, sometimes with tragic results. In fact because of their different training, designers and analysts have a different view of the same world, and sometimes they use a somewhat different terminology to describe the same problem.

The analyst himself is required to have a significant amount of experience. However regardless of his experience, the analyst is not able to guarantee the reliability and precision of the results he obtains. There is always a possibility that stresses are grossly underestimated. This fact strongly diminishes the reliability of FEM, and is the major reason for structural elements to be double checked with experimental techniques. This is particularly true in cases like

aircraft structures, where safety is a major objective. However experimental stress determination is very expensive and time consuming.



## Chapter II

### THE BLACK BOX APPROACH

The objective of this research is to create a software system which will allow the designer to use FEM without any understanding of FEM or any help from analysts. It should be underlined that such a new system is not intended to require any change in today's FEM theory or technology. What is sought is a way of implementing FEM which makes it easy to be used.

Since this new system is going to benefit the user it is advisable to define it first, strictly from the user interface viewpoint. The new system proposed (black box approach) should have these characteristics:

1. The geometry of the structure to be analyzed should be described with a CAD type of language. For example, if patches are used, the user should use a minimum number of them to properly describe the structure.
2. The user should be able to specify the precision with which stresses are to be computed all over the domain.<sup>1</sup> By precision all over the domain we mean that stresses should be

---

<sup>1</sup> Precision of displacements might be desirable. However their numerical values are normally of little interest to the designer. In any case with the Finite Element Method displacements are always much more precise than stresses.

approximated within a certain error of the exact solution not only at the best sampling points, but everywhere, without the use of stress smoothing techniques.

3. The output should be a color picture showing the stress intensity using one of the many criteria available (Tresca, Von Mises) [ 1 ], as specified by the user. The displacement field should also be shown.
4. The user should not need to be aware of what an element or a node is. The mesh description should not be required of the user since all the information that he needs are stresses and displacements. This means that when displacements or stresses are shown graphically, the user should not see the mesh but only those lines that define the structure geometrically, such as sharp edges or patch boundaries.

Requirements (1) and (2) above, imply that there has to be an algorithm which will automatically discretize the structure (automatic mesh generation) and will automatically refine the mesh, so that the specified precision will be reached. While automatic mesh generation has been successfully demonstrated, the manner of determining mesh refinement for a given precision requirement is still the object of intense research.

In the next chapter (chapter 3) a brief review of these research efforts is given. In chapters 4 and 5 a 2-D experimental software system developed during the course of this research and based on the black box approach, is described. The mathematical theory on which

the system is based is presented in chapter 6, while some examples to demonstrate the system capabilities are given in chapter 7. In chapter 8 the extension of this system for the static analysis of shell is discussed briefly, conclusions follow in chapter 9.

### Chapter III

#### SELF-ADAPTIVE ANALYSIS PACKAGES

In the last few years several researchers [ 8-19 ] have studied ways to create software packages that will automatically increase the number of degrees of freedom of a mesh in regions where the precision of the solution is poor. These systems are called self-adaptive analysis packages.

The algorithm devised for such packages are iterative in nature and they all have the same logical structure. These are the basic steps:

1. Run a first analysis using a trial mesh supplied by the user.
2. Identify the regions where the error is too large. If the error is below the specified value all over the domain, then exit.
3. Otherwise increase the number of degrees of freedom in the regions identified in step 2.
4. Run the analysis using the new mesh.
5. Go to step 2

The only differences among the available self-adaptive analysis packages are the criteria used in step 2 and the algorithms used in step 3.

Up to now several criteria have been proposed to determine automatically the accuracy of the solution. They all belong to one of the following four groups [ 14 ]:

1. A posteriori error estimate [ 10, 14, 18, 19 ].

This approach allows to determine the error of the solution for each element. The error in the solution or displacements is computed for each element in either energy or Sobolev norm. No equivalent error estimate for the derivative of the solution or stresses has been proposed. Furthermore an error bound for the solution in norm for each element does not translate into a pointwise error bound for the solution within the element.

2. Local measurements of residuals [ 15 ,18 ,19 ].

This approach does not relate directly to the error in displacement or stresses either. Furthermore its reliability can be questioned since this approach is directly related to the idea that the precision of the solution of a linear system of equations can be measured by the residual. However it is very well known that a small residual does not necessarily imply a small error in the solution itself.

3. Local test to determine how much improvement may be obtained from a new degree of freedom [ 11, 12 ].

In this approach a new degree of freedom is added and a local solution is carried out. The improvement in strain energy density is then computed. If the improvement is greater than a specified value, then the new degree of freedom is left in place, otherwise it is deleted. Again no relation is given between the error indicator and the precision of displacements

and/or stresses. Furthermore as shown in [ 16 ] it is possible that the existence of an orthogonality condition between the residual vector and the new degrees of freedom introduced, will give the false conclusion that the exact solution has been reached.

4. Measurement of strain energy density gradient [ 17 ].

In this approach an estimate of the number of degrees of freedom needed is derived by considering to the gradient of the strain energy density. It is assumed that the higher the gradients the more degrees of freedom are needed. Energy density however is not always a good parameter to be used since stress components in a region might vary significantly without any corresponding variation in stress energy density. A more appropriate parameter to be used are the stress components themselves and their gradients. Again no direct relation is provided between the error indicator and displacements or stresses.

Only two algorithms have been proposed for increasing the number of degrees of freedom (enrichment) in regions of the domain where the solution is poor [ 9 ].

The first is called H-convergence [ 10, 12, 13 ]. In this approach the elements are subdivided into smaller ones. Only one type of element is utilized, in two dimensions a triangle, in three dimensions a tetrahedra. The polynomial order of the trial functions or mode shapes used inside each element never changes (for each trial function there exists a degree of freedom).

The number of schemes proposed for subdividing elements is limitless. The only problem of H-convergence is in dealing with the transition zone between regions that are subdivided, and those that are not. Depending on how this problem is solved two different basic approaches can be defined.

In the first approach triangles in the transition zone are broken so that no node will be a corner node of a triangle and at the same time a mid-node of another triangle. In this way continuity requirements are automatically satisfied without any additional action. H-convergence is particularly handy when used here, since already existing analysis packages can be used for the analysis step. The only drawback is that the transition zone might contain elements whose shapes is far from optimal, from a computational viewpoint.

In the second approach no attempt is done to break the triangle in the transition zone. Continuity instead, is enforced by establishing a set of linear relations among nodes' displacements. However very few commercial analysis packages can handle these linear relations.

The other way to increase the number of degrees of freedom in a given region is called P-convergence [ 9, 11 ]. In this approach the number of elements remains unchanged. The only thing that is increased is the polynomial order of the modes shapes used in the elements themselves.

There are several drawbacks to P-convergence. The most severe is that the available mode shapes are limited and might not be sufficient to satisfy convergence. Also stresses must be computed

using stress smoothing techniques which reliability is not certain. Furthermore new software analysis packages tailored to this type of approach have to be developed.

Finally it should be noted that more sophisticated approaches have been proposed lately [ 16,18 ,19 ]. They combine both H and P-convergence and several of the criteria listed above to determine regions which must be enriched.



## Chapter IV

### A NEW EXPERIMENTAL SELF-ADAPTIVE SYSTEM

In the second chapter specifications were given for a new black box analysis system. These specifications are intended to shield the user from the problems facing today's FEM users and at the same time guarantee a high degree of reliability giving the user confidence in the results he has obtained.

In this chapter a new experimental two-dimensional system, tailored to the black box approach, will be introduced. This system spans only a fraction of all the possible applications of FEM in linear structural analysis. Still it should be realized that what it will be said for this small system can always be expanded to other more general systems.

These are the capabilities that the new system offers to the user:

1. It allows him to model 2-D structures (membranes) under plane stress conditions. Curved trusses are also available to model flanges. For example a wide flange beam can easily be modeled by using the plane stress capabilities for the web and trusses for the flanges.
2. It uses three and four-sided patches for modeling membranes. The four sided patches use complete cubic polynomial expansion plus two quartic terms. This is the same polynomial

expansion used for 2-D isoparametric twelve node elements. The three-sided patches use the complete cubic expansion except for the bilinear term.

3. Each patch must have constant thickness and material properties. Different patches can have different material properties and/or thicknesses.
4. Trusses can only exist on the boundary of a patch. Again each truss must have constant area and material properties. Different trusses can have different material properties and/or areas.
5. Geometric boundary conditions can only be applied at the patch vertices and edges. Displacement can be specified to be zero in the  $X_1$  or  $X_2$  direction or both. It is not possible to specify zero displacements in an oblique direction.
6. Loads can only be concentrated loads and line loads. Concentrated loads can only be applied at the patch vertices. Line loads can only be applied at the patch edges and they have to be constant along edges.

## Chapter V

### INTERNAL ORGANIZATION OF THE NEW SYSTEM

#### 5.1 ELEMENTS USED

The new system uses only two different type of elements: constant strain triangles for membranes under plane stress condition, and constant strain bars for trusses.

The constant strain triangle (CST) has been sometimes criticized [ 4 ] for its poor performance in certain situations (e.g. bending of a beam), when compared to higher order elements. This is true when the comparison is based only on the number of degrees of freedom used. However when the overall computational effort [ 6 ] is considered (which includes stiffness matrix computation and assembly, number of degrees of freedom, and most important stiffness matrix band-width) then the different in performance is not so obvious [ 5 ]. Furthermore CST's are very reliable elements which can easily take any kind of distortion and not give unreasonable stress values at the nodes like higher polynomial elements do. This last characteristic was a strong reason for choosing the CST.

The two nodes truss element was an obviouse choice to model flanges, since it has to be coupled with the CST.

## 5.2 INITIAL MESHING

The initial meshing is done by approximating four-sided patches by two triangles and three-sided patches by one triangle. In the case of three-sided patches the three vertices are connected with straight lines. In the case of the four-sided patches, first the patch is transformed into a quadrilateral by connecting the four vertices with four straight lines, then the closest opposite vertices are connected with a straight line too. This is done in order to minimize triangles distortion.

Each flange is initially modeled with a single truss bar.

## 5.3 ENRICHMENT ALGORITHM

Since the new system uses only one type of element for each type of structural member, the only enrichment algorithm that can be used is H-convergence.

In this specific case, the algorithm is identified by the following basic features:

1. The enrichment is done by splitting already existing triangles. Already existing nodes are not relocated or destroyed.
2. The location of any new node will be computed in parametric space and then mapped into real space. The parametric space is the same parametric space which defines the patch where the new node belongs. This feature guarantees that the more the mesh is refined the better it will be approximating the patches' boundaries.

3. The splitting algorithm has been designed so that all nodes will be at the corners of triangles and none at the mid-point of any triangle edge. Thus no special relation need be imposed among degrees of freedom.

The enrichment algorithm receives the triangles which, based on some error indicator, have been already marked when the solution is not precise enough (see Fig. 1). The algorithm then goes through the following steps.

1. Split all the marked triangles into four triangles as shown in figure 2.
2. Identify all the triangles which have at least one edge adjacent to two edges of two different triangles (non conforming-edge), as shown in figure 3, and split each one into four triangles (see Fig. 4).
3. Repeat step 2, as shown in figure 5 and 6.
4. Mark all the triangles which have at least one or more non-conforming edges such that none of their nodes lie on a non-conforming edge of adjacent triangles, (see Fig. 7, 9, and 11). If none exist stop, else continue.

5. For each triangle marked in step 5 perform the following steps (see Fig. 8, 10, and 12). If all the three edges are non-conforming or if the longest edge is conforming while the other two are not, then split the triangle into four triangles. In all other cases, split the triangle into two triangles creating a mid-node on the longest edge.
6. Go to step 4

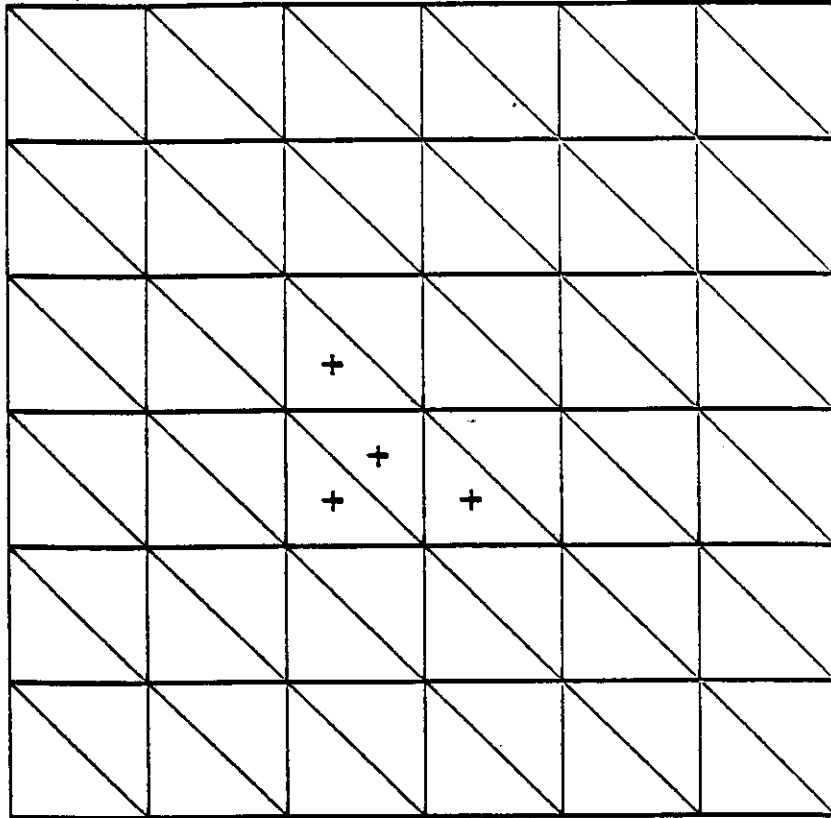


Figure 1: Triangles marked to be split

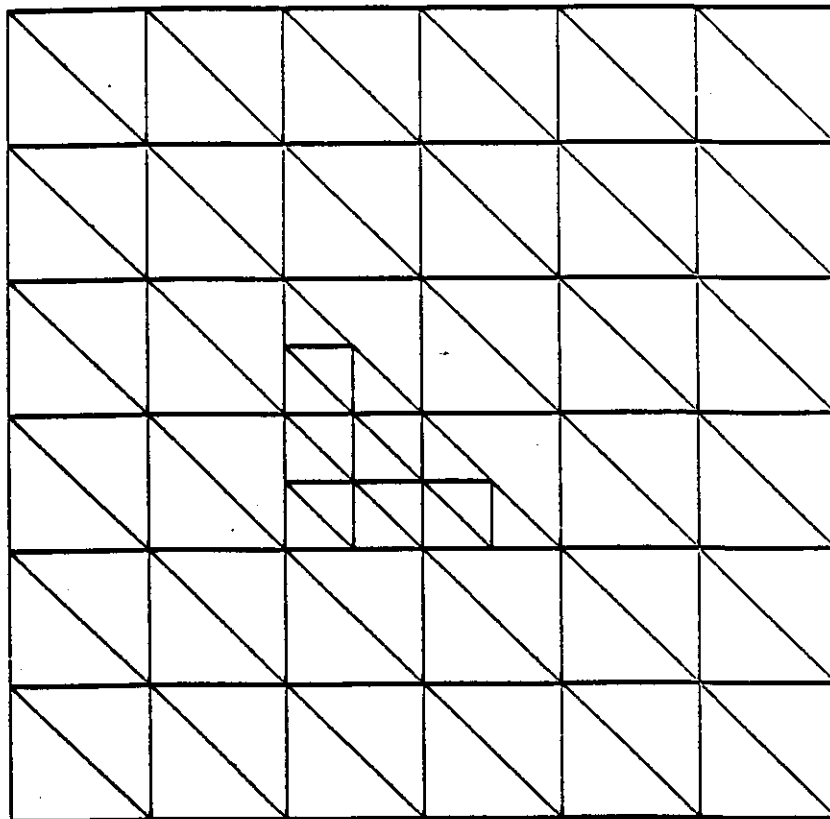


Figure 2: Triangles after splitting in step 1



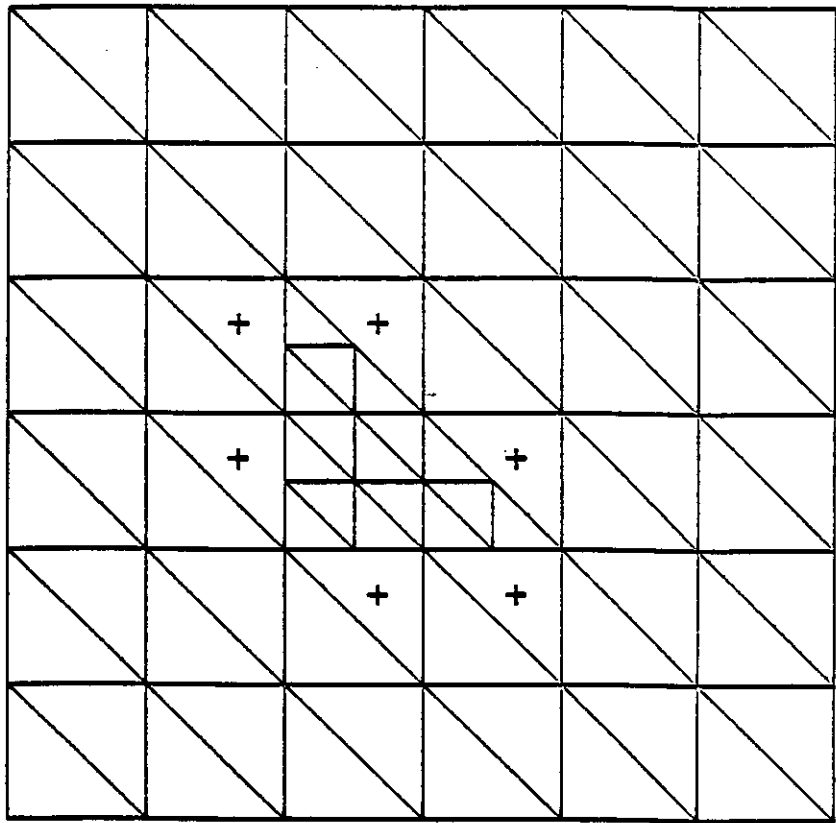


Figure 3: Triangles marked to be split in step 2

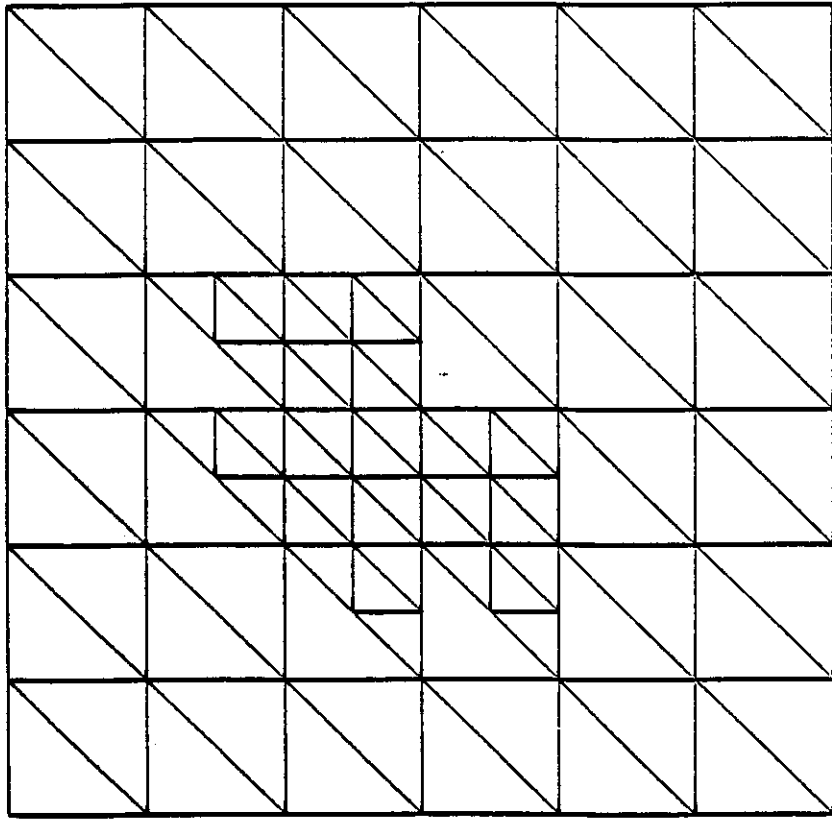


Figure 4: Trinangles after splitting in step 2

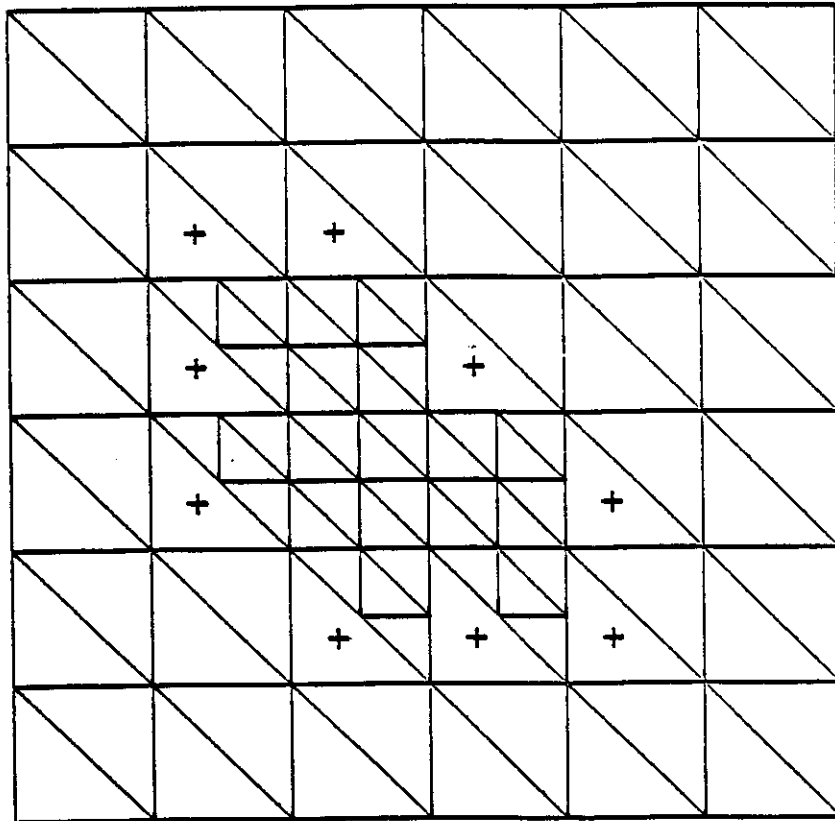


Figure 5: Triangles marked to be split in step 3

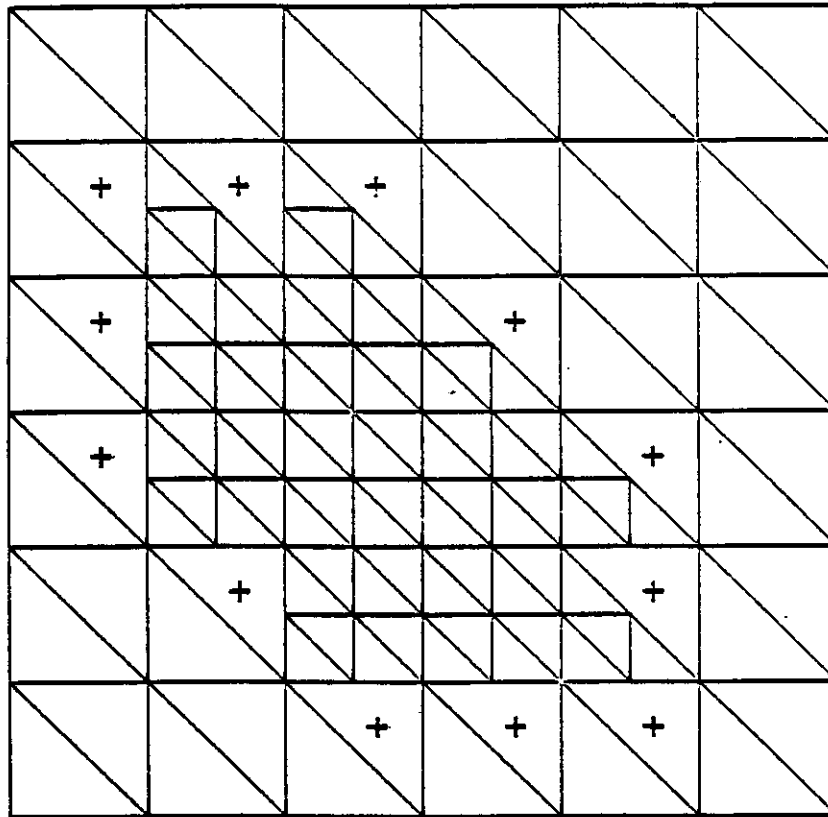


Figure 7: Triangles marked to be split in step 4 (first pass)

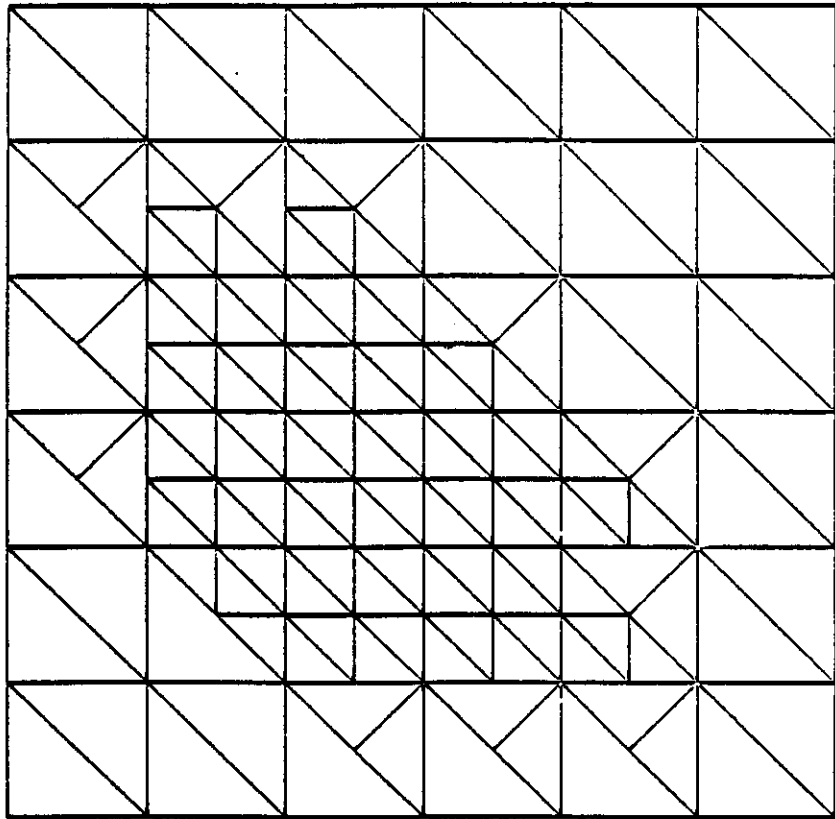


Figure 8: Triangles after splitting in step 5 (first pass)

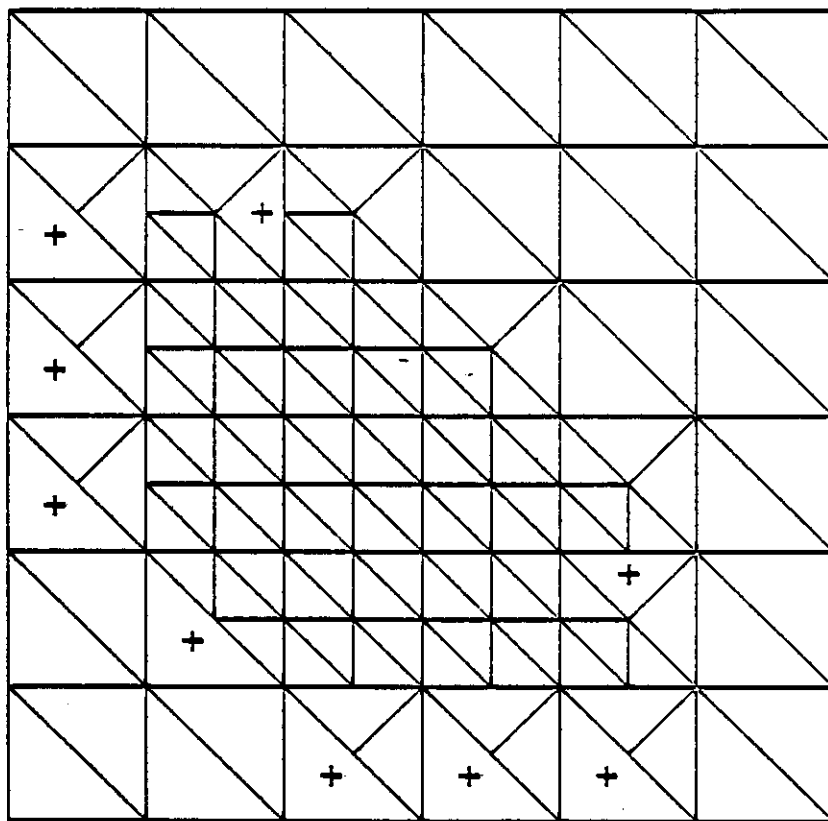


Figure 9: Triangles marked to be split in step 4 (second pass)

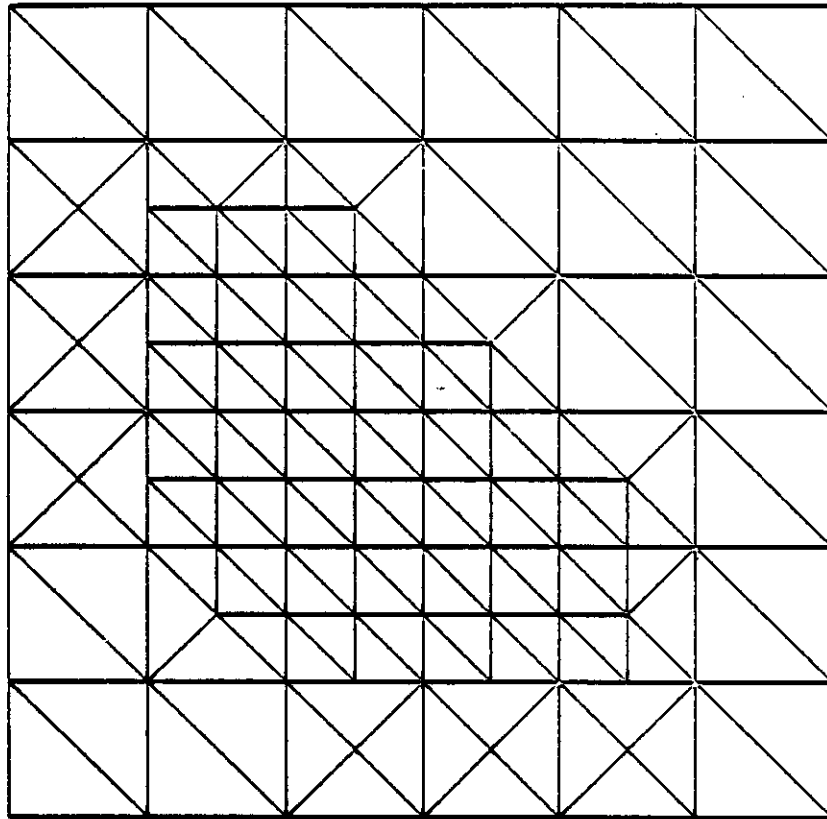


Figure 10: Triangles after splitting in step 5 (second pass)

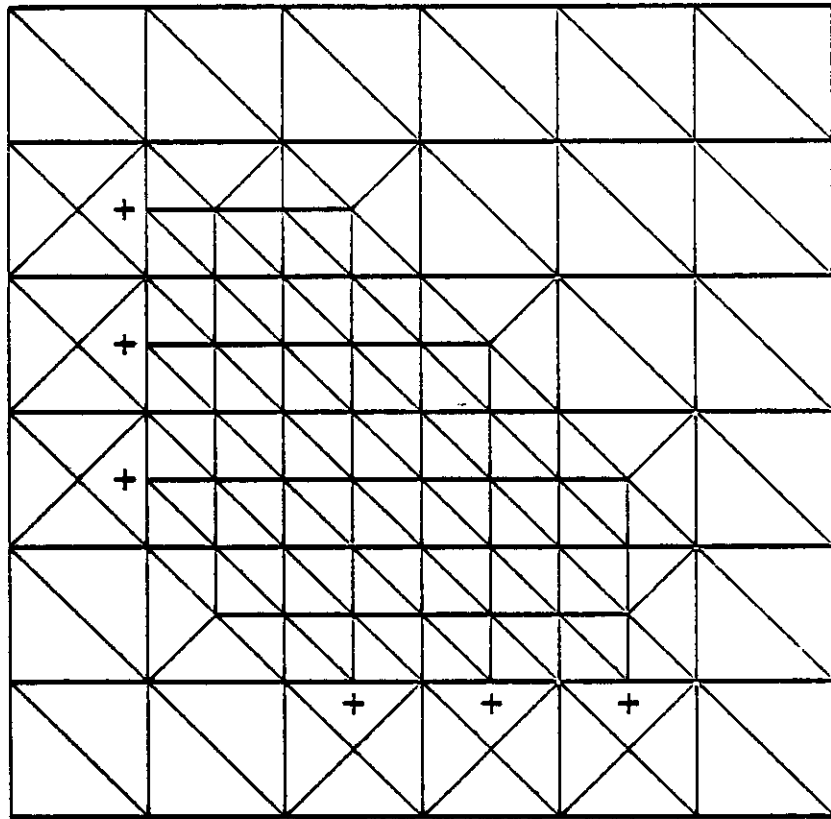


Figure 11: Triangles marked to be split in step 4 (third pass)



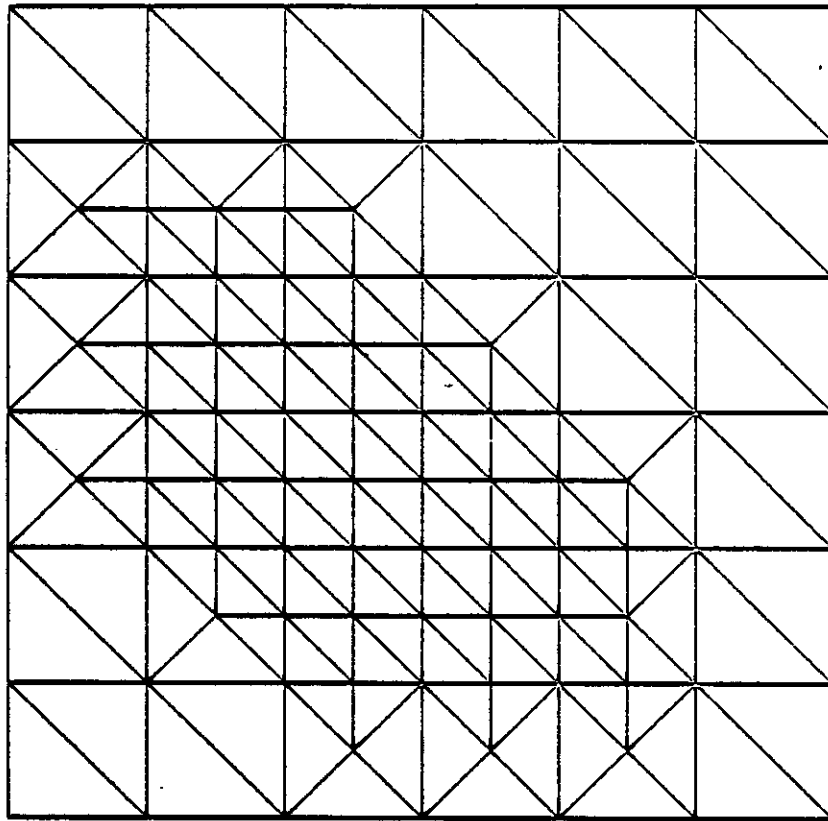


Figure 12: Triangles after splitting in step 5 (third pass)

In steps 1,2 and 3 the triangles are split in a way that does not increase distortion. In steps 2 and 3 a buffer zone is created to make sure that the area initially marked for splitting, will be fully enclosed in the area of split triangles. A more specific reason will be given in the next chapter.

From step 3 on, the transition area is created. The transition area denotes the area of triangles which are between unsplit triangles and split ones. This area is mostly composed of triangles which have been generated by splitting initial triangles into two.

This part of the algorithm has been designed so as to minimize the increase in triangle distortion within the transition area. For example, if initially all the triangles have angles of 90, 45 and 45 degrees as shown in figure 1, then at the end of the splitting, all triangles still have angles of 90, 45 and 45 (see fig. 12).

In step 3 the condition that the triangles have to satisfy in order to be marked for splitting, has been introduced to avoid the possibility that a non-conforming edge will be facing more than two triangles as shown in the sequence from figure 13 through figure 15. If this happens, then the criterion for splitting given in step 4 is no longer valid.

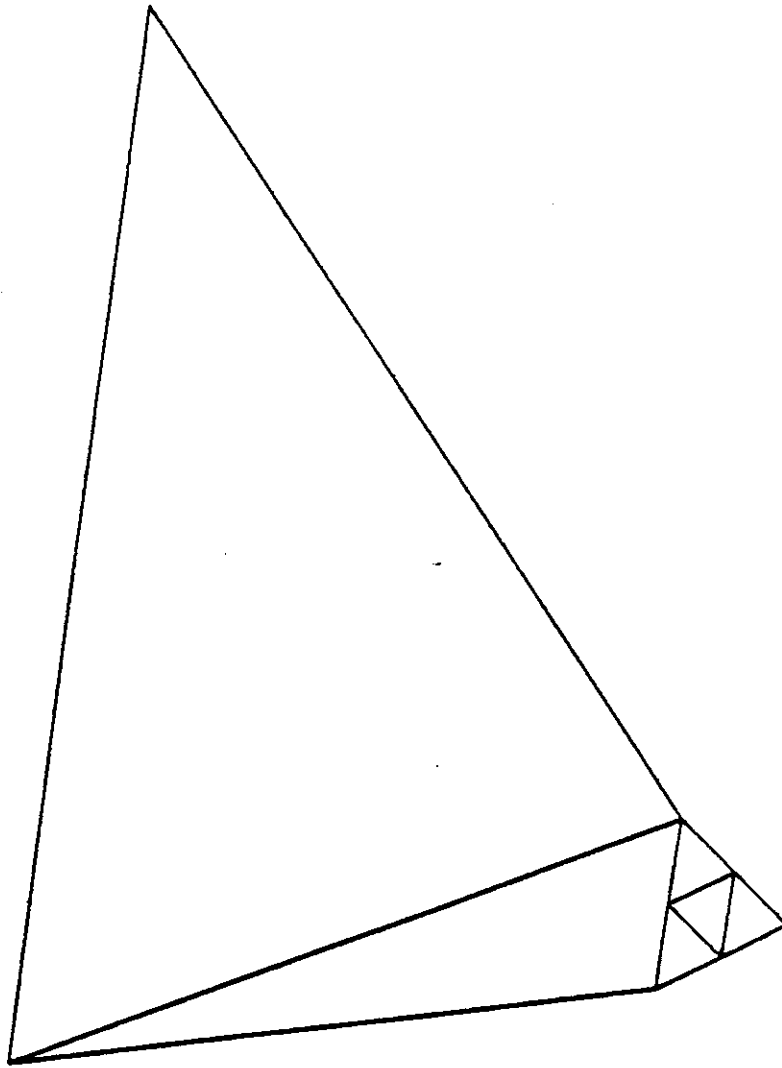


Figure 13: Non-conforming edge facing more than two triangles (frame1)

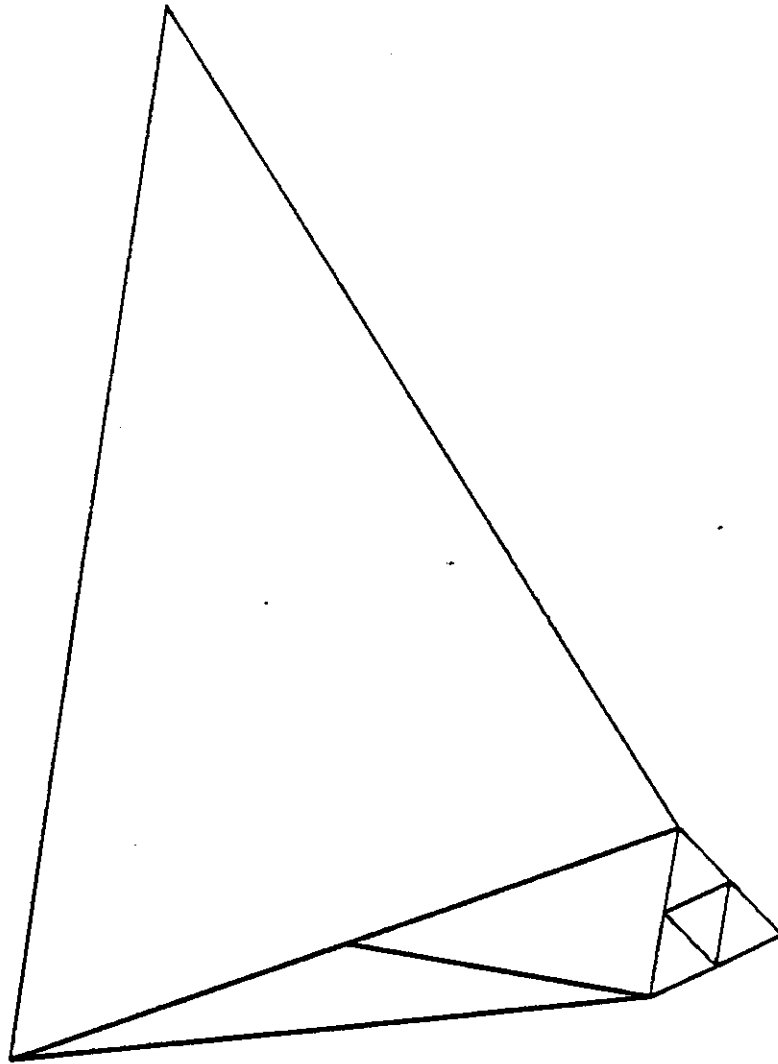


Figure 14: Non-conforming edge facing more than two triangles (frame2)

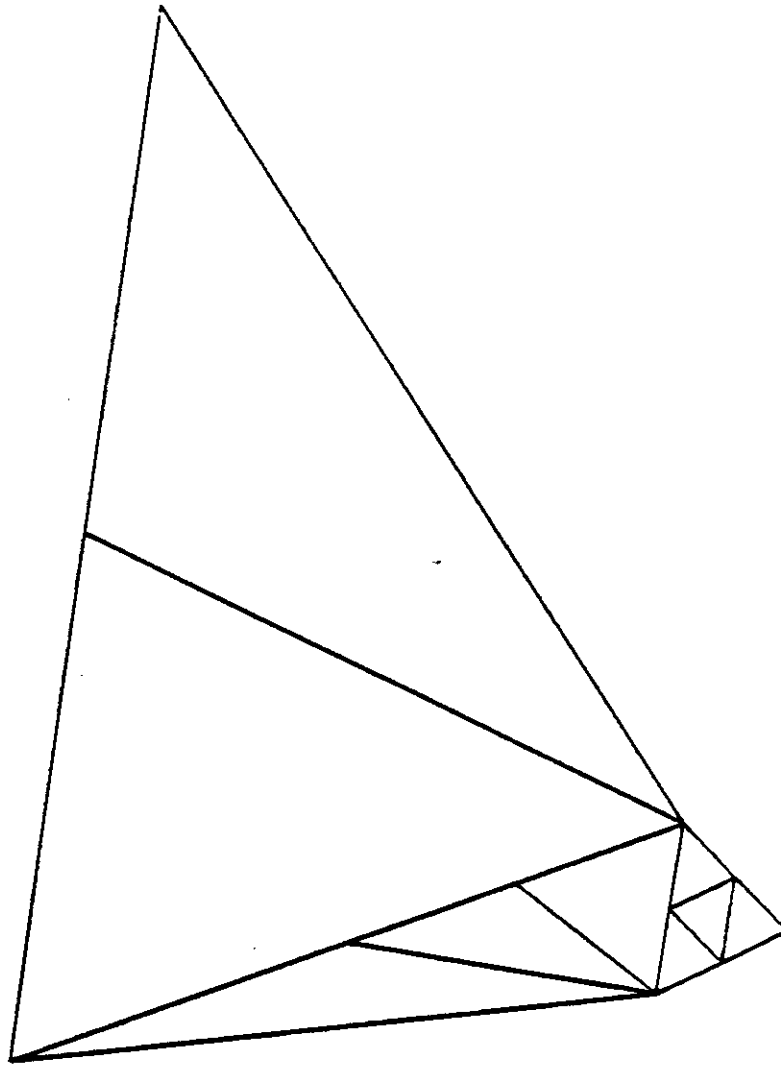


Figure 15: Non-conforming edge facing more than two triangles (frame3)

The algorithm can never come to deadlock. The fact that in step three triangles which do not have vertices on an adjacent triangle non-conforming edge will not be marked for splitting, means that they will have to be split in coming cycles. It might appear at first that a circular type of deadlock might happen, in which triangle A is waiting for triangle B to be split, triangle B is waiting for triangle C to be split and, triangle C is waiting for triangle A to be split. Such a case cannot happen since splitting always takes place at the longest edge. Thus if the chain of locks starts from a given triangle, it must start from the longest edge. In order to continue, the longest edge of the previous triangle must not be the longest of the actual one. Thus there is no way that the locking chain can travel back to the triangle it started from.

In general the splitting is done in the patch parametric space and the distortion of the elements is dependent on the distortion of the patches themselves. If the patch is a square then there is no difference between parametric space and Cartesian space since there is no distortion. In general to avoid potential problems, the distortion of the patches can be checked at the beginning by computing the Jacobian at some strategically located sampling points.

## 5.4 CRITERIA USED FOR THE ERROR INDICATOR

The criterion which determines the regions where the solution is not accurate enough is based on a direct calculation of the rate of convergence of the stresses for each element.

### 5.4.1 Criteria used for truss bars

Let us consider a single truss bar for simplicity. After the analysis the bar will have a given axial stress, constant all along its length. Then the triangles adjacent to the bar will be split which will in turn force the bar to be divided into two new bars. The stress value of the new bars will be initialized to the stress value of the old bar. When the analysis is run again the new computed stress for each new element will be compared with the old one. If the difference is above the error tolerance specified by the user, then the triangles adjacent to the truss bar will be marked for splitting. The bars themselves are never marked for splitting since, as previously stated, flanges can only exist on the boundaries of patches, and never float alone in space.

### 5.4.2 Criteria used for triangles

Extending the criterion presented in the previous section to triangles is straightforward. Again let us consider a single triangle belonging to a 2-D structure. After the analysis is carried out the triangle holds the stress values which are constant throughout the triangle itself. If the triangle is arbitrarily marked for splitting then the

enrichment algorithm will automatically split the triangle into four as shown in figure 1 and 2. The stress values for the new triangles are initialized to the stress values of the parent triangle. When the analysis is carried out again the new stress values of the new elements can be compared to the old values. This comparison of the stresses can be carried out in norms. This means that given the old stresses  $\tau_{ij}$  and the new stresses  $\sigma_{ij}$  it is possible to define a difference stress tensor  $\delta_{ij}$  as

$$\delta_{ij} = \sigma_{ij} - \tau_{ij} \dots \dots \dots (5.1)$$

Finally we can compute the norm  $\|\delta_{ij}\|$  of the difference stress tensor as:

$$\|\delta_{ij}\| = (\delta_{ij} \delta_{ij})^{1/2} \dots \dots \dots (5.2)$$

The norm  $\|\delta_{ij}\|$  is invariant with respect to the orientation of the cartesian axis.

The triangle will or will not be marked for splitting depending on the value of this norm. If the norm  $\|\delta_{ij}\|$  will be bigger than the error tolerance specified by the user, then the triangle will be marked for splitting, otherwise it will not.



It should be noted that the criterion proposed here is completely different from all previously proposed criteria since it requires the results of two consecutive analysis. Instead, all criteria proposed until now use the results of only one analysis, and in some cases require additional local analysis to determine if the element or area under consideration should be enriched.

## 5.5 OVERALL SYSTEM ORGANIZATION

The system is composed of three modules: a preprocessor, a self-adaptive package, and a postprocessor.

The preprocessor reads in the data in card image format; it does extensive error checking and also checks that the patches are not too distorted. Finally it reorganizes the data in a new format, ready to be fed into the self-adaptive module.

The self-adaptive module performs the actual analysis. It goes through the following steps.

1. Call the analysis routine for the first analysis.
2. Mark all triangles to be split.
3. Split triangles that are marked for splitting.
4. Call the analysis routine for the next analysis
5. Locate the triangles where the stress variation is bigger than the error tolerance, and mark them for splitting.
6. Locate the truss bars where the stress variation is bigger than the error tolerance, and mark the adjacent triangles for splitting.

7. If no triangle has been marked, then exit, else go to step 3.

These steps are shown in the flowchart of figure 16.

The postprocessor generates several pictures. One of these shows the structure in the undeformed and deformed position at the same time. Another picture shows the color code of stress levels computed using either the Von Mises or Tresca criteria. Since no stress smoothing technique is used, the color remains the same within each triangle.

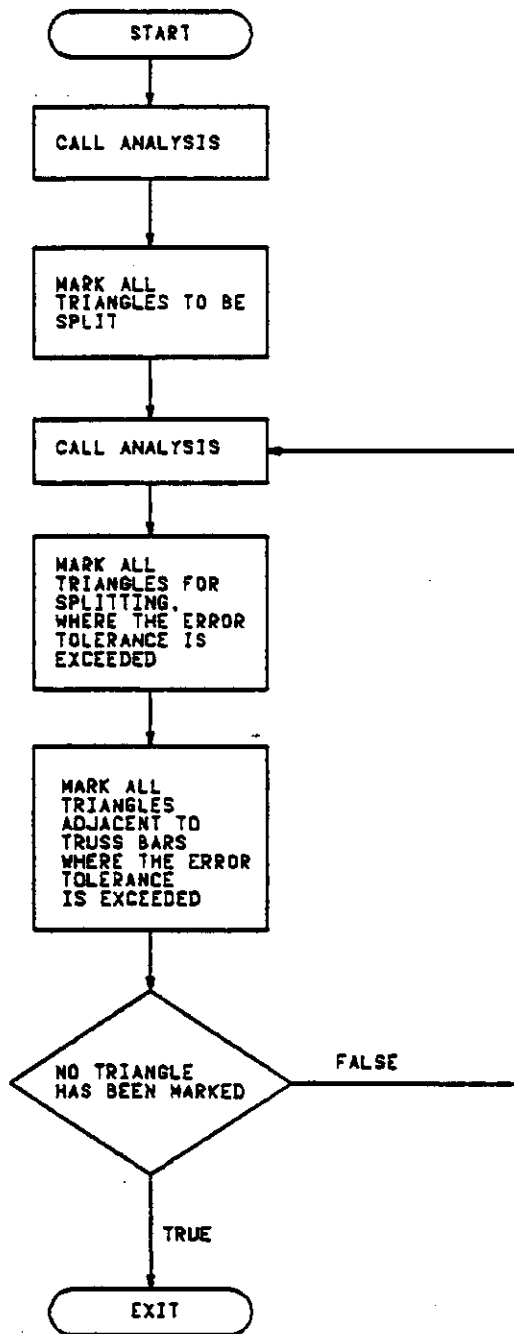


Figure 16: System flowchart

## Chapter VI

### ERROR ESTIMATE OF STRESSES

In the introduction we said that one of the most important features of a self-adaptive system is that it allows the user to specify directly the precision required for stress calculations.

In the previous chapter it was said that precision of the stresses is "acceptable" once the new criterion presented is met.

In this chapter it will be shown that, if this criterion is met, the precision of the stresses all over the domain is smaller or equal to the error tolerance, without the use of any stress smoothing techniques.

#### 6.1 ERROR ESTIMATE OF AXIAL STRESS IN TRUSS BARS

Let us consider a single bar (one dimensional problem) before and after it has been divided into two bars. If the bar is very small it can be assumed that:

1. The point generated to split the bar, lies in the middle of the two end points of the bar. This is not normally true since the point is generated in the parametric space, however if the bar is very small compared to the overall patch to which it belongs, any discrepancy due to the patch distortion becomes negligible.

2. The stress at midpoint, which is the optimum sampling point for stress evaluation within the bar [ 4 ], is equal to the exact solution at that point.
3. The exact solution for the stresses will vary linearly along the bar (see figure 17 top). This means that the error of the stresses is zero at the midpoint, and is maximal and equal in magnitude at both end points.

The same assumptions are also valid for the two new bars obtained by dividing the original one (see figure 17 bottom).

Based on these assumptions it can be said that after two analysis the exact solution is known both at midpoint and quarter points of the old bar (midpoints for the new bars).

If only one of the two new bars is considered, it is easy to see that the maximum error in stress is equal to the difference between the constant value produced from the second analysis and the value of the exact solution at both end points. In particular the error at the end point, which is also the midpoint of the old bar, can be easily computed, and is equal to the difference between the stress value produced from the first analysis in the old bar and the stress value produced from the subsequent analysis in this new bar. This difference is exactly the error tolerance specified by the user and introduced in the previous chapter. Finally since the errors at both end points are equal, it can be concluded that the error in the stress in all truss bars is always less than or equal to the error tolerance, once the criterion presented in the previous chapter is met.

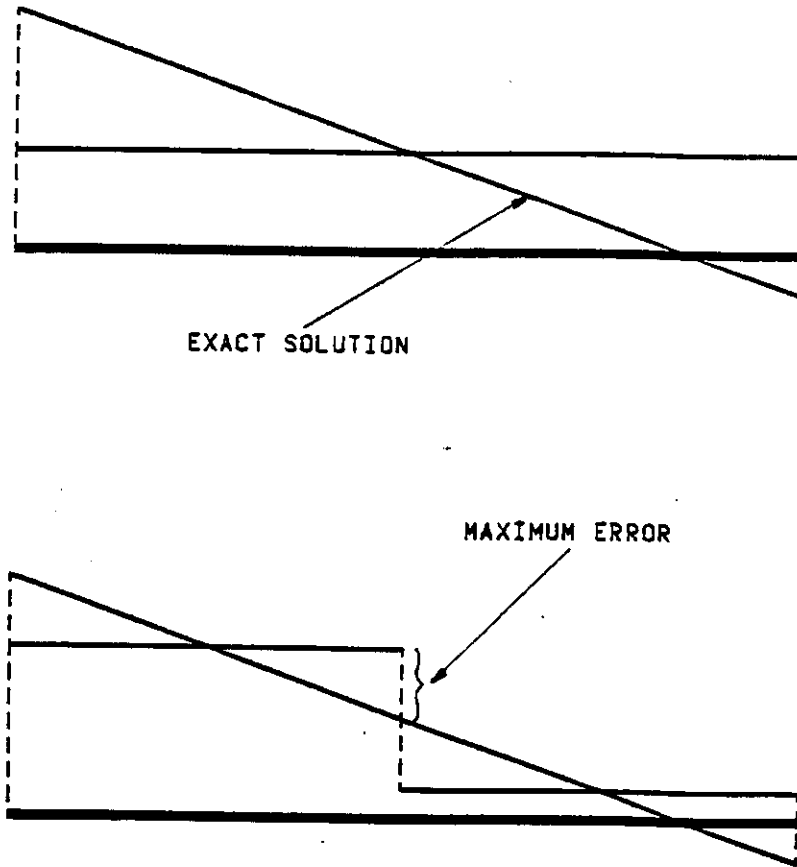


Figure 17: Error estimate in truss bars

## 6.2 ERROR ESTIMATE OF STRESSES IN TRIANGLES

### 6.2.1 Basic assumptions

The assumptions made for truss bars, when they are small enough, can also be extended to triangles (two dimensional problem), provided these are also small enough. The assumptions are as follows:

1. The points generated during the splitting effectively lie on the midpoints of the sides of the triangle.
2. The stresses at the centroid of the triangle (best sampling point) are essentially equal to the exact solution at that point [ 4 ].
3. The functions describing the stress components are all linear functions in  $X_1$  and  $X_2$ , and can be visualized as planes.

These assumptions are also valid for the four new triangles generated when the old one is divided into four triangles, a central one (central triangle) and three around it (adjacent triangles) shown in figure 18

Furthermore, as long as assumption 1 is true, the three adjacent triangles are equal, and they are the mirror image of the central triangle, and stress values for the old triangle are equal to stress values of the new central triangle since their centroids coincide.

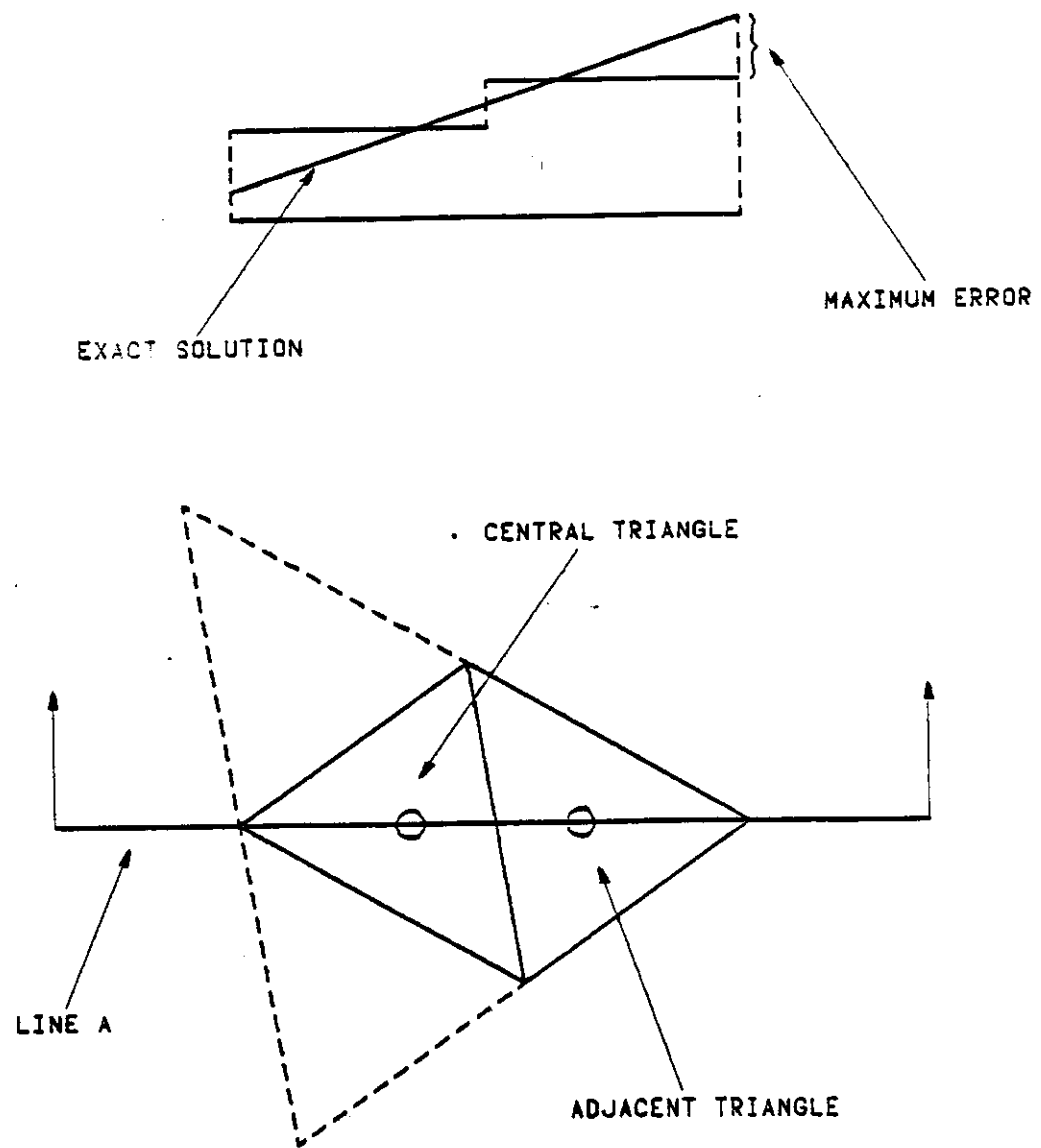


Figure 18: Error estimate in triangles



### 6.2.2 The error stress tensor

The error stress tensor  $\varepsilon$  is defined as:

$$\varepsilon_{ij} = \sigma_{ij}^* - \sigma_{ij} \dots \dots \dots (6.1)$$

where  $\sigma_{ij}^*$  is the exact stress tensor and  $\sigma_{ij}$  is the approximate value obtained from the last analysis.

Since each component of  $\varepsilon_{ij}$  is the result of the difference of a planar function and a constant function, it will be a planar function itself within all four triangles. This implies that, within each triangle, the maximum value in magnitude, of each component of  $\varepsilon_{ij}$  will be at one of the corners. Furthermore this function will be zero at each centroid and have the same slope in the  $X_1$  and  $X_2$  directions in all four triangles since the planar function used in the difference is the same for all four triangles. Considering these properties and recalling that all the adjacent triangles are equal, it can be said that the value of  $\varepsilon_{ij}$  at the same corner of all the adjacent triangles is the same. Also since the central triangle is the mirror image of all the adjacent triangles, the value of  $\varepsilon_{ij}$  at any corner of all the adjacent triangles will be equal in magnitude and opposite in sign to the value of  $\varepsilon_{ij}$  at the mirror corner of the central triangle.

The norm  $\|\varepsilon_{ij}\|$  is defined as:

$$\|\varepsilon_{ij}\| = (\varepsilon_{ij} \varepsilon_{ij})^{1/2} \dots \dots \dots (6.2)$$

Its value is independent from the  $X_1$ - $X_2$  axis orientation.

### 6.2.3 Error estimate

Let us now consider only the central triangle and any one of the three adjacent triangles. These two triangles have been drawn with continuous line in figure 18. Line A has been drawn passing across the centroids of both triangles. Recalling that one triangle is the mirror image of the other, it can be seen that:

1. The new line always passes through the opposite nodes of the two triangles.
2. The distance between the two centroids is one third of the distance between the two opposite corners.
3. The point of intersection of the new line and the edge shared by the two triangles is also the midpoint of both the opposite corners and the two centroids.

In figure 18 the approximate value of a stress component, resulting from the second analysis, and the exact solution are shown along line A. The approximate value is an horizontal line within each triangle, while the exact solution is an oblique line.

Both errors at the opposite corners are equal in magnitude (as stated above). Their value is equal to the difference of the constant stress component in the two triangles. Combining this and the fact that the stress components obtained from the first and second analysis for the central triangle are equal, it can be seen that the error for each stress component in any adjacent triangle at the corner opposite to central triangle is equal to the difference between the same stress component computed in the two last analysis.

If norms are considered then it can be stated that the error stress norm  $\|\varepsilon_{ij}\|$  in any adjacent triangle at the corner opposite to the central triangle is equal to the norm  $\|\delta_{ij}\|$  of the difference stress tensor.

Furthermore, recalling that for each component of  $\varepsilon_{ij}$

$$\varepsilon_{ij} \leq \|\varepsilon_{ij}\| \dots \dots \dots (6.3)$$

we can say that in each adjacent triangle

$$\varepsilon_{ij} \leq \|\delta_{ij}\| \dots \dots \dots (6.4)$$

where  $\varepsilon_{ij}$  is evaluated at the corner opposite to the central triangle.

Let us now define  $\|\delta_{ij}\|_m$  as the largest of the three norms  $\|\delta_{ij}\|$  in the adjacent triangles ( $\|\delta_{ij}\|$  in the central triangle is always zero). Recalling what has been stated in the previous section and because of equation 6.4 we can say that the absolute value of any component of  $\varepsilon_{ij}$  in all four triangles is always less than or equal to  $\|\delta_{ij}\|_m$ . Also whenever  $\|\delta_{ij}\|_m$  is larger than the error tolerance, all four triangles will be split because of steps 2 and 3 in the splitting algorithm. Thus it can be concluded that if convergence has been reached, then the error in all stress components will be less than or equal to the error tolerance.

### 6.3 PRECISION OF ERROR ESTIMATE OF STRESSES

In the previous two sections the error computations for stresses are based on several assumptions. The most important are that the exact solution for stresses is linear in  $X_1$  and  $X_2$  within each element and that the error of the stresses at the centroid of any triangle is negligible compared to the error at the corners. Both assumptions are never exactly true and thus a certain error exists when  $\epsilon_{ij}$  is estimated.

In the case of one dimensional problems it is possible, by taking advantage of superconvergence, to prove that at any point the asymptotic ratio  $r$  between the true error and its estimate is given by the expression (see Appendix A)

$$r = (n-1)n/(2^n-1) \dots \dots \dots (6.5)$$

where  $n$  is the degree of the first non zero polynomial term of the Taylor expansion at that point. If  $n=1$  then the ratio  $r$  is one. This means that at any point which is not a point of stationary value for the exact solution of the axial stress the error estimate is asymptotically exact. If  $n>1$  then the solution is stationary at the point under consideration. In the case  $n=2$  which occurs most often, the ratio  $r$  is equal to  $5/3$ . It should be noted that the number of points where  $n>1$  is always finite.

It is also possible to prove (see Appendix A) that the factor by which the error estimate asymptotically decreases at each iteration is  $2^n$ . Thus all points where  $n>1$  can be detected by looking at the way the error estimate varies from one iteration to another.

Some numerical tests have also been run for the one dimensional case. The tests have been carried out by analyzing a truss bar under several combinations of loads and boundary conditions. The structure was at the beginning discretized with a single bar and then at each iteration all the bars were split into two. The exact solution was always available. The results perfectly match with equation 6.5 and they consistently show that at points where  $n > 1$  the ratio  $r$  approaches the values given by equation 6.5 from below as the element size decreases. This means that values given by equation 6.5 when  $n > 1$  can be considered for practical purposes an upper bound.

For example one of the tests consists of a truss bar of length  $\pi$  pinned at both ends and under the distributed load  $\sin(x)$ . The governing equation is

$$u_{,xx} = \sin(x) \quad u(0)=u(\pi)=0 \quad \dots \dots \dots (6.6)$$

The exact solutions for the displacements and stresses are

$$u = \sin(x) \quad \dots \dots \dots (6.7)$$

$$u_{,x} = \cos(x) \quad \dots \dots \dots (6.8)$$

Because of symmetry the analysis has been carried out only for  $0 \leq x \leq \pi/2$ . Error underestimation has been monitored at  $x=0$ ,  $x=\pi/4$ , and  $x=\pi/2$ . The initial mesh consists of two equal length elements instead of one in order to include the gridpoint  $x=\pi/4$  from the beginning. The elements in subsequent meshes are all of equal

length. The values of  $r$  in the neighbourhood of the three points for increasingly smaller elements length are listed in table 1.

TABLE 1  
Example of Error Underestimation (1-D)

Length	$r$ at $X=0$	$r$ at $X=\pi/4$	$r$ at $x=\pi/2$
$\pi/4$	1.605	1.605	1.082
$\pi/8$	1.651	1.189	1.020
$\pi/16$	1.663	1.078	1.005
$\pi/32$	1.666	1.036	1.001
$\pi/64$	1.667	1.017	1.000
$\pi/2048$	1.667	1.001	1.000

As it can be seen at  $x=0$   $r$  converges to  $5/3$  from below since  $n=2$ . At the other two points  $n=1$  and  $r$  converge to 1. At  $x=\pi/2$  it does so faster since the first order term of the Taylor series at that point is much larger than the higher order terms. In fact the second order term is zero. A similar study in 2-D is not possible since superconvergence does not exist. However as shown in the next chapter, it turns out that in practice underestimation of the true error is not a problem from an engineering viewpoint, and it does not affect the reliability of the system.

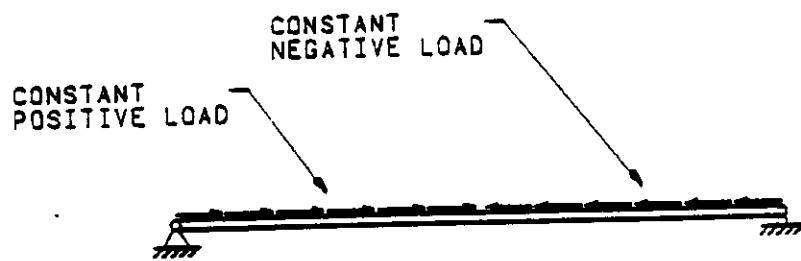
A refinement of the algorithm in order to minimize the possibility of underestimation of the true error would be to monitor the rate at which the error estimate decrease for each triangle and truss bar from one iteration to another. Based on this information a safety

factor could be introduced when the error estimate is compared to the error tolerance.

#### 6.4 FALSE CONVERGENCE

False convergence happens when after a few iterations the algorithm stops and the precision of stresses is far below the one specified. This might happen for example when the new mode shapes introduced by splitting the triangles are orthogonal to the load vector [ 15 ]. In figure 19 such a case is show for a one dimensional problem. The resulting axial stresses in all elements in the first and second iteration are the same. This is interpreted by the program as the fact that the exact solution has been reached even though it is far from it since the stress distribution for this case is piecewise parabolic.

False convergence has never been noticed during the course of this research. The reason of this is that the system in its actual configuration allows only for constant loads along the edges of the triangles initially used. It is expected that even linearly or quadratically varying loads along the edges should not give any problem since these loads have a strong component in the generalized direction of the new mode shapes created by splitting triangles. However additional testing is necessary to support this statement.



ITERATION 1



ITERATION 2

Figure 19: Case of false convergence



## 6.5 TREATMENT OF SINGULARITIES

In certain cases, stress distribution in a structure can reach an infinite value at certain points which are called singularity points. This can happen because of concentrated loads applied to the structure, or because of the existence of sharp reentrant corners in the structure itself. In either case, regardless of how small the triangles can be, as long as they have finite dimensions, the error at singularity points will always be infinite.

This fact is of importance only to mathematicians but not to designers or engineers since it is very well known that singularity points are only a mathematical abstraction, as well as concentrated loads or sharp reentrant corners. However the system itself is not aware of these facts and will try to solve the mathematical problem. It will keep splitting triangles close to the singularity points and never be able to stop.

To avoid this possibility the user has the option of specifying a maximum number of iterations. If nothing is specified the default value of 8 is used. If this limit is met the user has the option to restart execution for a new round of iteration. Also to help him making such a decision the postprocessor has the option of displaying the area where convergence has not been reached.

## Chapter VII

### COMPUTER IMPLEMENTATION AND EXAMPLES

#### 7.1 COMPUTER IMPLEMENTATION

The new system described in the previous chapters has been implemented on the IBM 3033 at UCLA running under the OS/MVS operating system. The preprocessor and the self-adaptive package are written in PLI. The postprocessor is partly written in PL/I and partly in FORTRAN. The overall size of the three modules is about 4000 lines.

The input to the preprocessor is a card image file. Even though it is expected that the input to the preprocessor would be generated automatically by a CAD system, the actual input language has been designed so that it would be as user friendly as batch input can be. The input is free format and comments can be added by putting an asterisk as the first card character. The amount of data that has to be keyed in has been reduced to a minimum, and extensive error checking is provided by the preprocessor.

The capabilities of the system can be best demonstrated through some examples.

## 7.2 EXAMPLE NO. 1

The first example consists in the analysis of a rectangular plate with a circular hole under tension as shown in figure 20.

The thickness of the plate is 0.1 inches and the material properties are:

Young modulus 10,000 ksi,

Poisson ratio 0.25,

yield stress 30 ksi.

Since both the structure and the loading are doubly symmetric, the analysis has been run only for one quarter of the plate as shown in figure 21. The same figure also shows the patches used for modeling the structure. The small triangles represent the center point of each patch in the parametric space. The input file is 25 lines long. The initial mesh is shown in figure 22.

The error tolerance has been specified as 10% of the yield stress (3 ksi). Convergence has been reached in 7 iterations. The final mesh is shown in figure 23 and it consists of:

875 nodes,

1706 degrees of freedom,

1611 triangles.

Color coded stress levels based on Von Mises criterion are shown in figure 24. The lowest stress level is blue, the highest is red.

The exact solution to the problem is available in series form [ 7 ]. The series gives precise results only at points which distance from the origin is less than 10 inches. The accuracy of the algorithm has

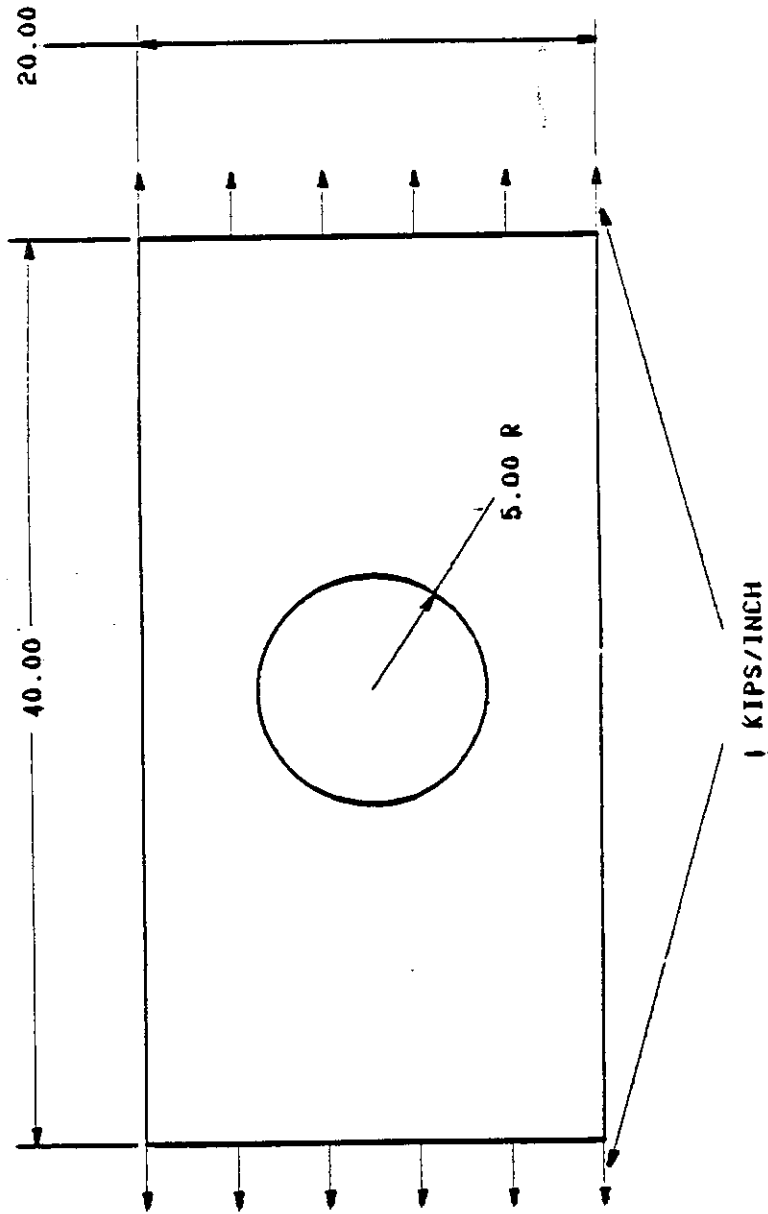


Figure 20: Example no. 1, description of the problem

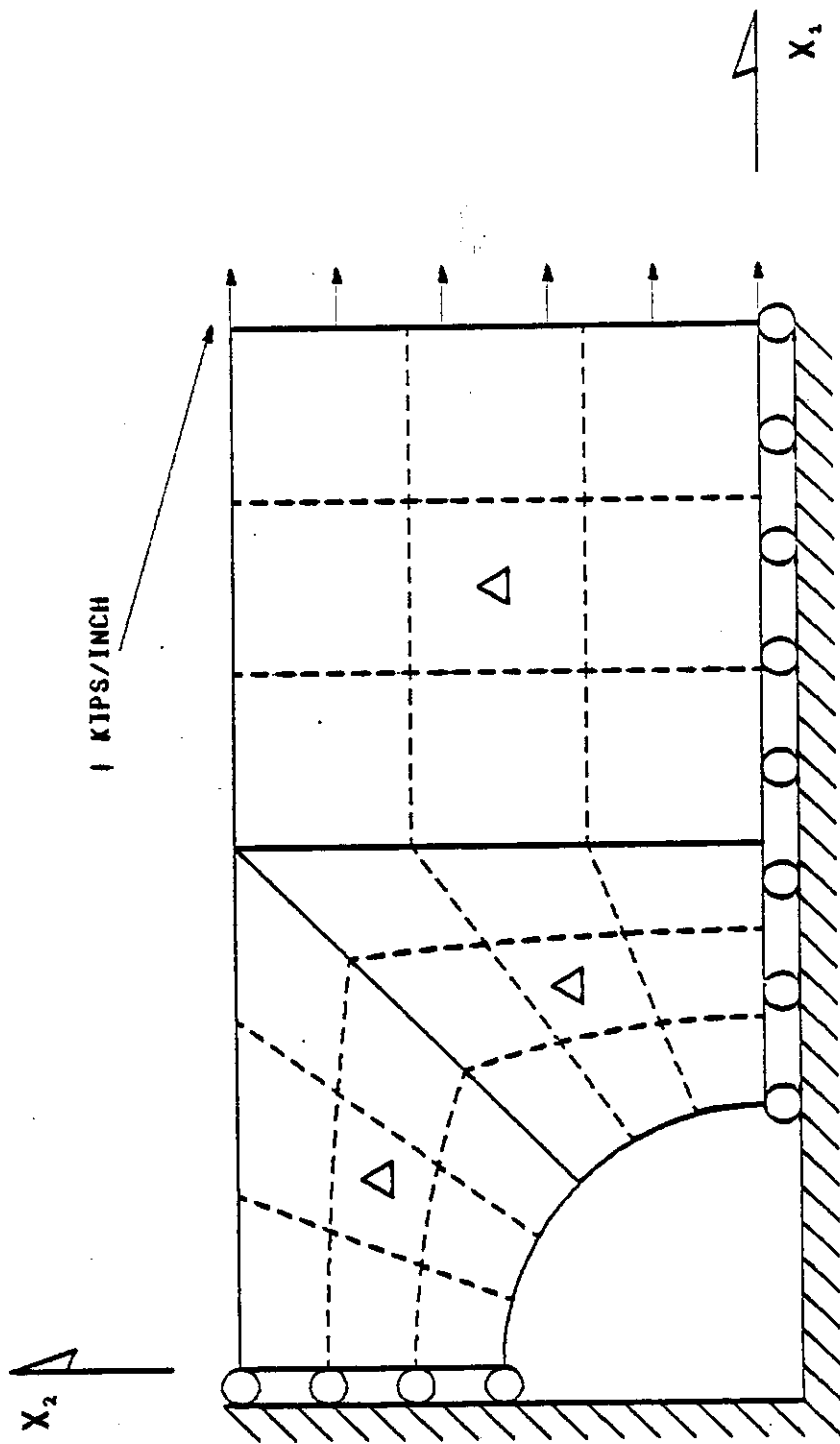


Figure 21: Example no. 1, input to the system



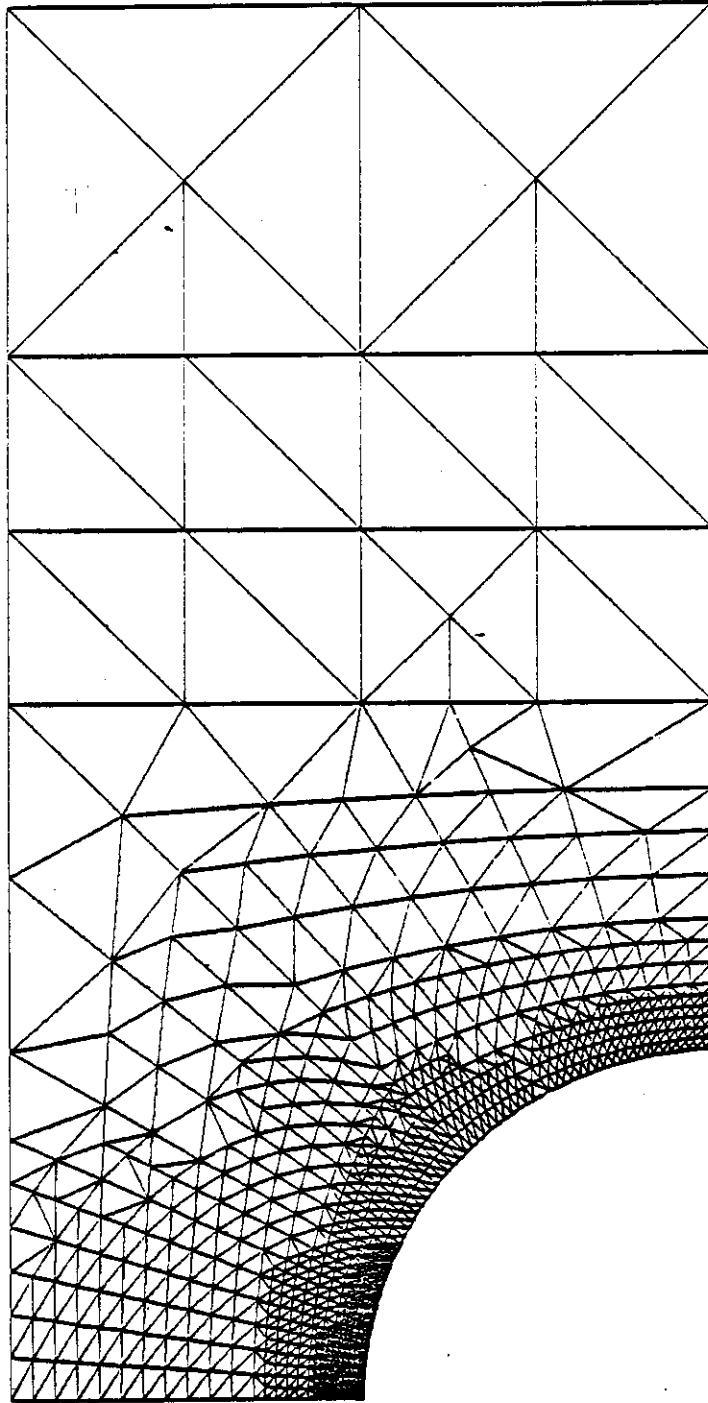


Figure 23: Example no. 1, mesh at iteration 7

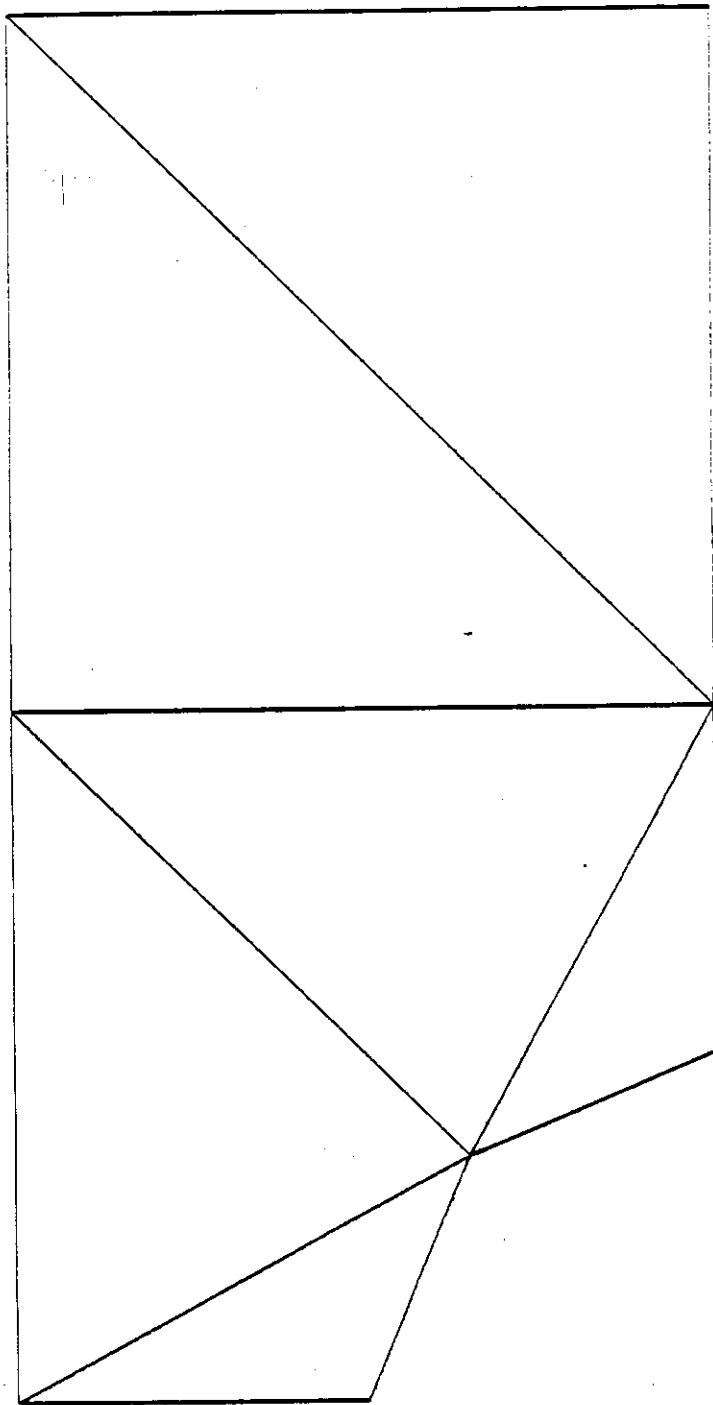


Figure 22: Example no. 1, mesh at iteration 1



been check in this example by comparing the close form solution with the FEM solution in the area where the exact solution is valid. The comparison has been carried out by computing, for all triangles within 10 inches from the origin, the error stress tensor norm at each corner. This procedure was based on years of experience which have consistently shown that the maximum error of stresses within a constant strain triangle is at one of the corner. It results that nowhere in the area under consideration the error stress tensor norm is larger than the error tolerance (3 ksi). In table 2 the four highest error stress tensor norms found are listed. In the first two columns the points coordinates are given, in the third column the values of the norm are given.

TABLE 2

Example no. 1, Highest Error Stress Tensor Norms  
(Error Tolerance 3 ksi)

$X_1$	$X_2$	$\ \epsilon_{ij}\ $
3.536	3.536	2.544
2.347	4.415	2.519
2.975	4.019	2.510
2.874	4.091	2.504

It can be seen that the error stress tensor norm at all points is well below the error tolerance.

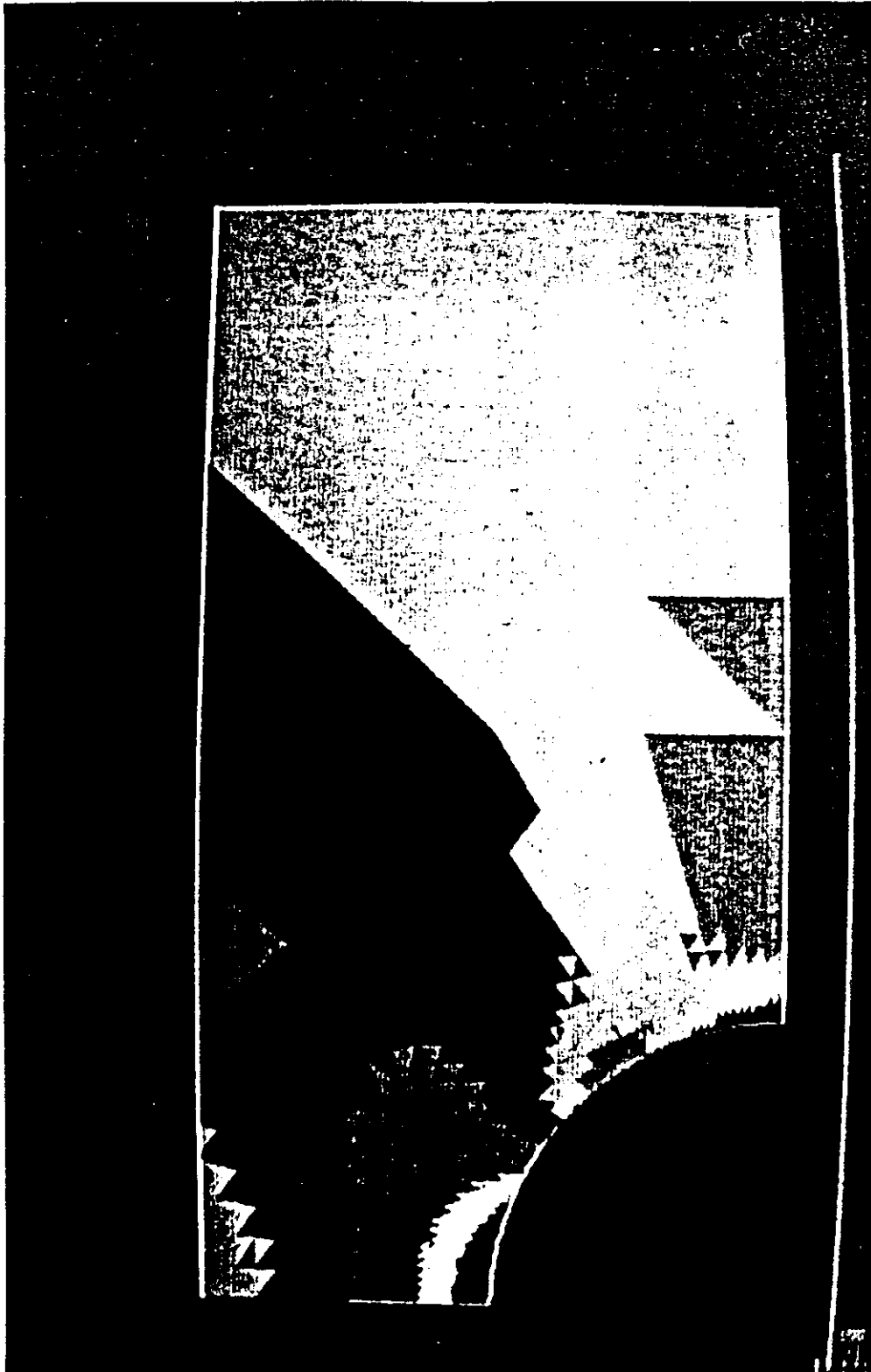


Figure 24: Example no. 1, color coded stress levels

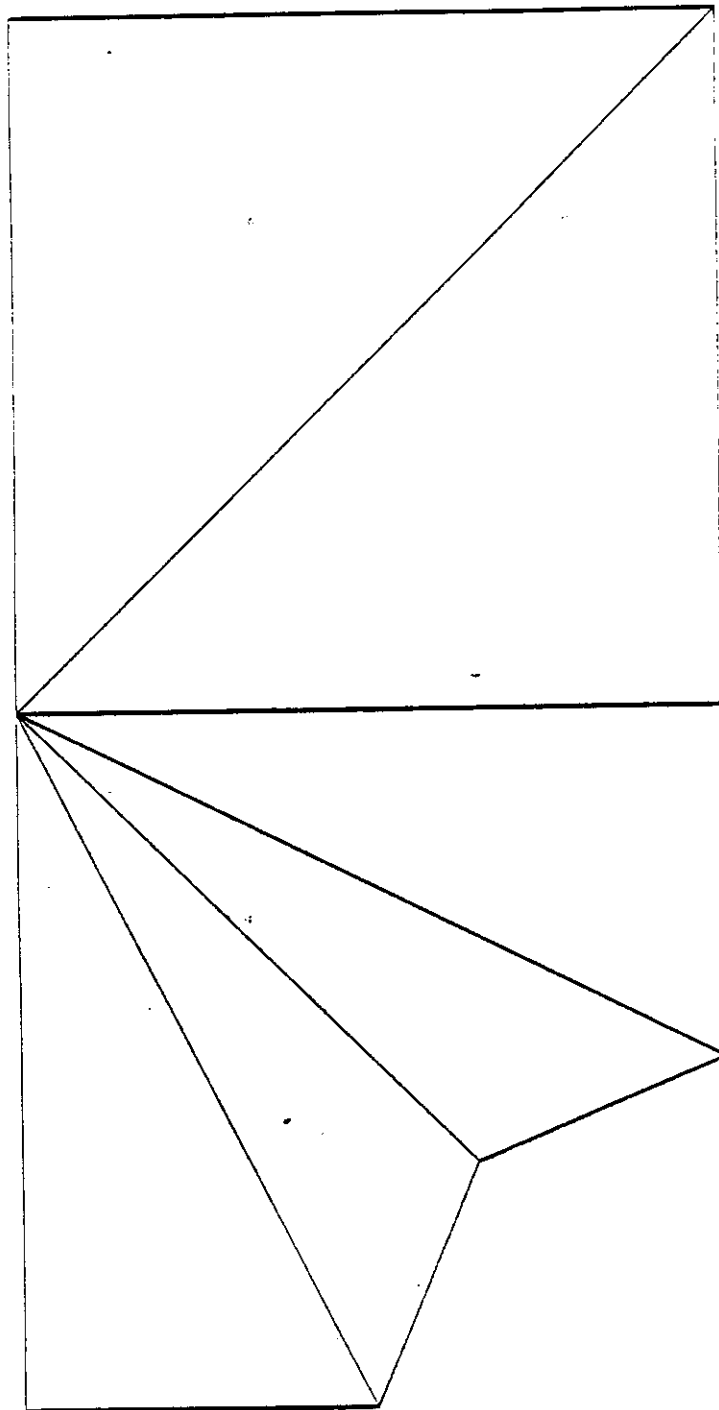


Figure 25: Example no. 1, initial mesh, second run

The same example has also been run by altering the initial meshing of all the four-sided patches. The quadrilaterals defined by the patches' vertices were split into triangle along the longest diagonal instead of the shortest as shown in figure 25. The initial triangles as well as those generated by subsequent splitting are more distorted than those used int the first run.

Convergence has been reached in 8 iterations. One more iteration than in the first run is needed because the distortion of the triangles has a negative effect on the precision of the solution. The final mesh is shown in figure 26 and it consists of:

1277 nodes

2508 degrees of freedom

2397 triangles.

A comparison of the two final meshes shows that in some areas where the triangles are very distorted, additional mesh refinement is needed. This is consistent with the fact that distortion decrease precision.

The accuracy of the solution has been checked again to see how sensitive the algorithm is to to a change of initial mesh. The comparison has been carried out exactly as for the first run. At two triangles at one corner each the error stress tensor norm was larger than 3 ksi. The two corners sit on the boundary of the hole. Their coordinates and distance from the origin is given in table 3. In tables 4 and 5 the value for the exact and approximate stresses as well the error stress tensor and its norm are given for both points.

TABLE 3  
Corners Coordinates

Case no.	$X_1$	$X_2$	$(X_1^2 + X_2^2)^{1/2}$
1	2.665	4.223	4.994
2	2.769	4.157	4.995

TABLE 4  
Stresses at Corner, Case 1  
(Error Tolerance 3 ksi)

---	i=1, j=2	i=2, j=2	i=1, j=2	Norm
$\sigma_{ij}^*$	14.797	5.975	-9.405	---
$\sigma_{ij}$	14.260	4.114	-7.600	---
$\epsilon_{ij}$	.537	1.861	-1.805	3.204

TABLE 5  
Stresses at Corner, Case 2  
(Error Tolerance 3 ksi)

---	i=1, j=2	i=2, j=2	i=1, j=2	NORM
$\sigma_{ij}^*$	13.290	5.971	-8.907	---
$\sigma_{ij}$	13.016	3.984	-7.259	---
$\epsilon_{ij}$	.274	1.987	-1.648	3.075

As can be seen in the worst case (case 1) the error stress tensor norm is 3.204 ksi and exceeds the error tolerance (3 ksi) by 7%.

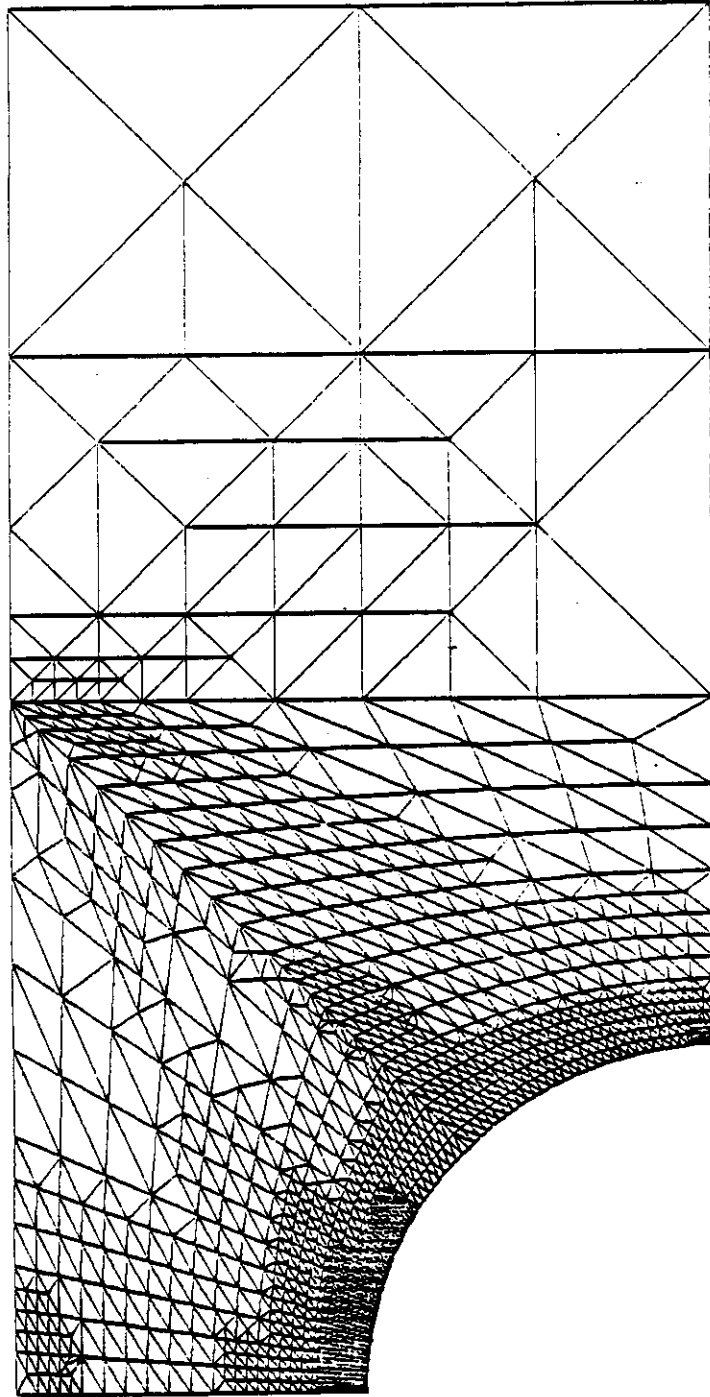


Figure 26: Example no. 1, final mesh, second run

TABLE 7

Stresses at Corner, Case 1  
(Error Tolerance 3 ksi)

---	i=1, j=2	i=2, j=2	i=1, j=2	Norm
$\sigma_{ij}^*$	14.840	5.913	-9.342	---
$\sigma_{ij}$	14.260	4.114	-7.600	---
$\epsilon_{ij}$	.580	1.799	-1.742	3.105

TABLE 8

Stresses at Corner, Case 2  
(Error Tolerance 3 ksi)

---	i=1, j=2	i=2, j=2	i=1, j=2	Norm
$\sigma_{ij}^*$	13.334	5.915	-8.858	---
$\sigma_{ij}$	13.016	3.984	-7.259	---
$\epsilon_{ij}$	.318	1.931	-1.599	2.990

imperfection in the geometric description of the model and how much is due to the algorithm itself.

It can be concluded that this example indicates that the precision of the final solution is essentially independent from the initial mesh used.

This result can be explained in part by the fact that the rim of the hole, which is a circle, was approximated by two spline curves. The effects of this approximation are that the two points under considerations lie at a distance from the origin (also the center of the hole) less than 5 inches.

A more consistent comparison has been done for these two points by ideally moving them along the line that connect them to the origin so that they will exactly lie on the rim of the hole. The new coordinates of the two points are shown in table 6. The results of the new comparison are shown in tables 7 and 8.

TABLE 6  
Corners Coordinates

Case no.	$X_1$	$X_2$	$(X_1^2 + X_2^2)^{\frac{1}{2}}$
1	2.668	4.228	5.000
2	2.772	4.161	5.000

As can be seen the error stress tensor norm at one of the of the corners (case 2) is less than the error tolerance. At the other corner the error stress tensor norm is 3.105 ksi and it exceeds the error tolerance (3 ksi) by 3%. Part of this error however can be justified by the fact that since a thin layer of material has been added to the hole, stresses on the rim tend to be slightly in error. It is however difficult to say how much of the whole error is due to the



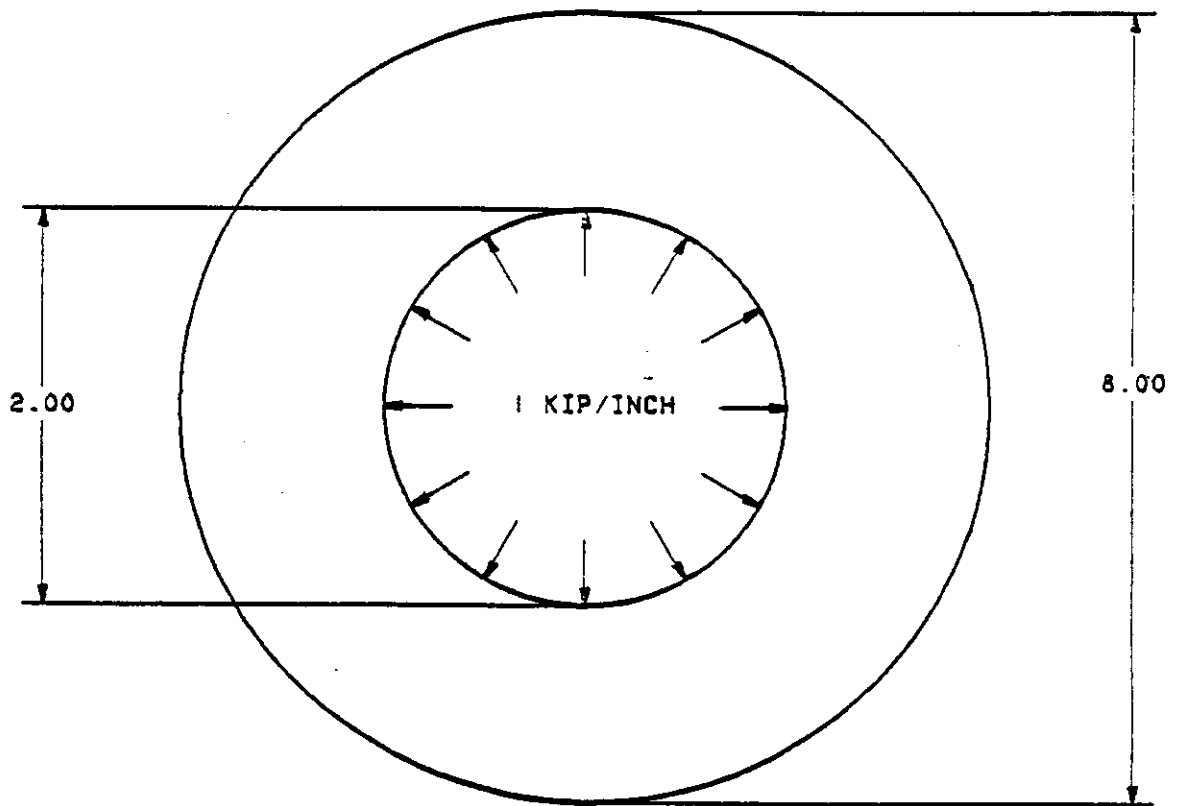


Figure 27: Example no. 2, description of the problem

### 7.3 EXAMPLE NO. 2

The second example consists of the analysis of a thin circular disk with a hole in the middle as shown in figure 27.

The thickness of the plate is 0.1 inches and the material properties are:

Young modulus 30,000 ksi,

Poisson ratio 0.3

yield stress 21 ksi.

The load consists of a uniform pressure applied to the hole boundary.

Since both the structure and the loading are doubly symmetric, the analysis has been run only for one quarter of the disk as shown in figure 28.

The same figure also shows the patches used for modeling the structure. Two four-sided patches are used. The small triangles represent the center point of each patch in the parametric space. The input file is 24 lines long. The initial mesh is shown in figure 29.

The error tolerance has been specified as 1.5 ksi which is about 7% of the yield stress. Convergence has been reached in 7 iterations. The final mesh is shown in figure 30, and it consists of:

1498 nodes,

2950 degrees of freedom,

2824 triangles.

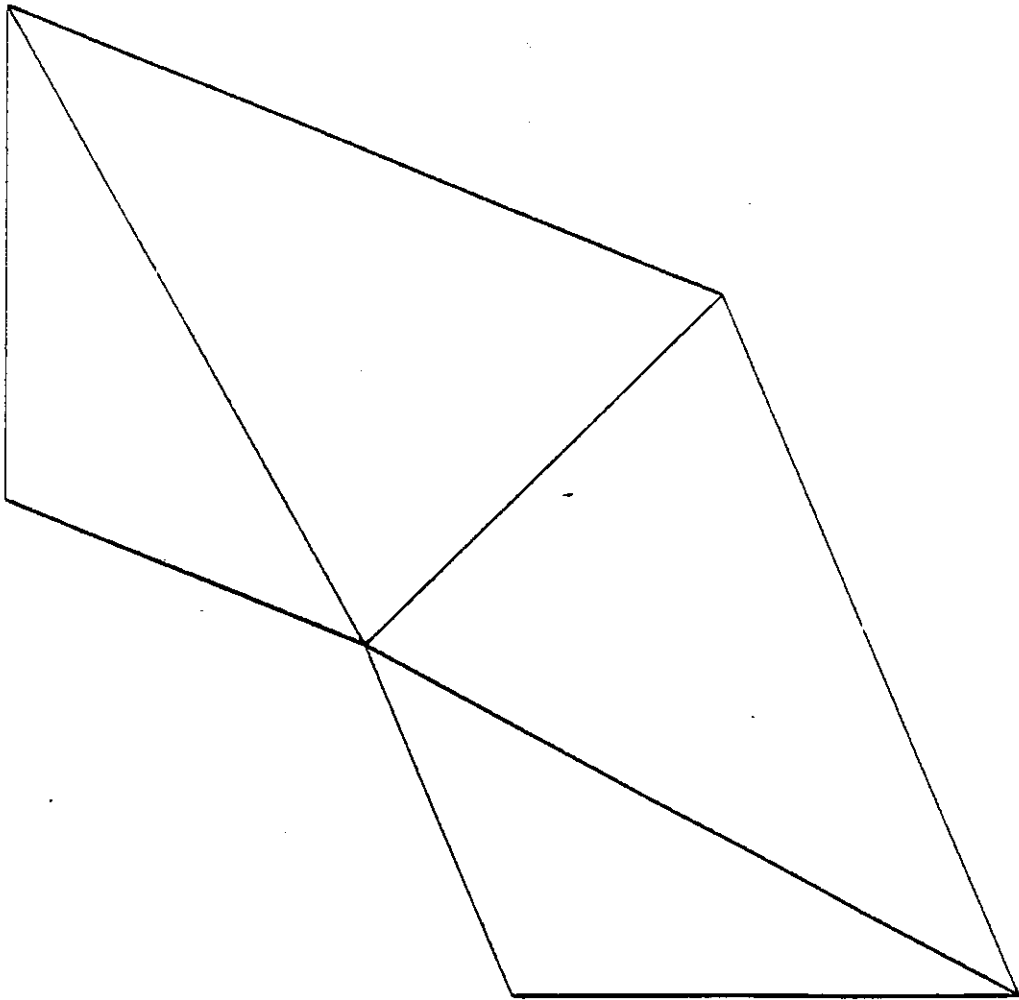


Figure 29: Example no. 2, mesh at iteration 1

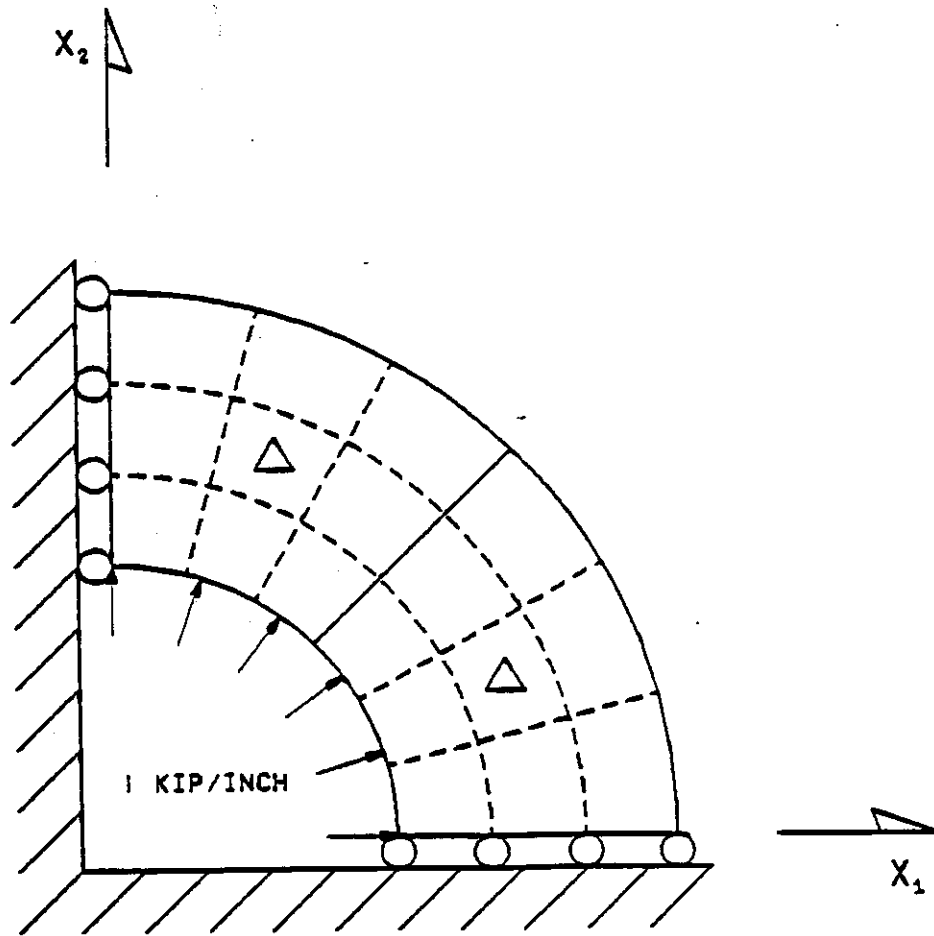


Figure 28: Example no. 2, input to the system

Even though the solution is point symmetric with respect to the origin, the final mesh does not have this type of symmetry. This is due to the fact that when the model is initially discretized this type of symmetry is lost. Still the final mesh is very close to being point symmetric with respect to the origin.

Color coded stress levels based on Von Mises criterion are shown in figure 31. The lowest stress level is blue, the highest is red.

Since the exact solution is available [ 2 ], the precision of the numerical results has been checked as in the previous example by comparing the exact solution with the numerical one at each corner of all triangles. It turns out that nowhere the error stress tensor norm is larger than the error tolerance (1.5 ksi). In table 9 the four highest error stress tensor norms found are listed. In the first two columns the points coordinates are given, in the third column the values of the norm are given.

It can be seen that the error stress tensor norm is at all points is well below the error tolerance.

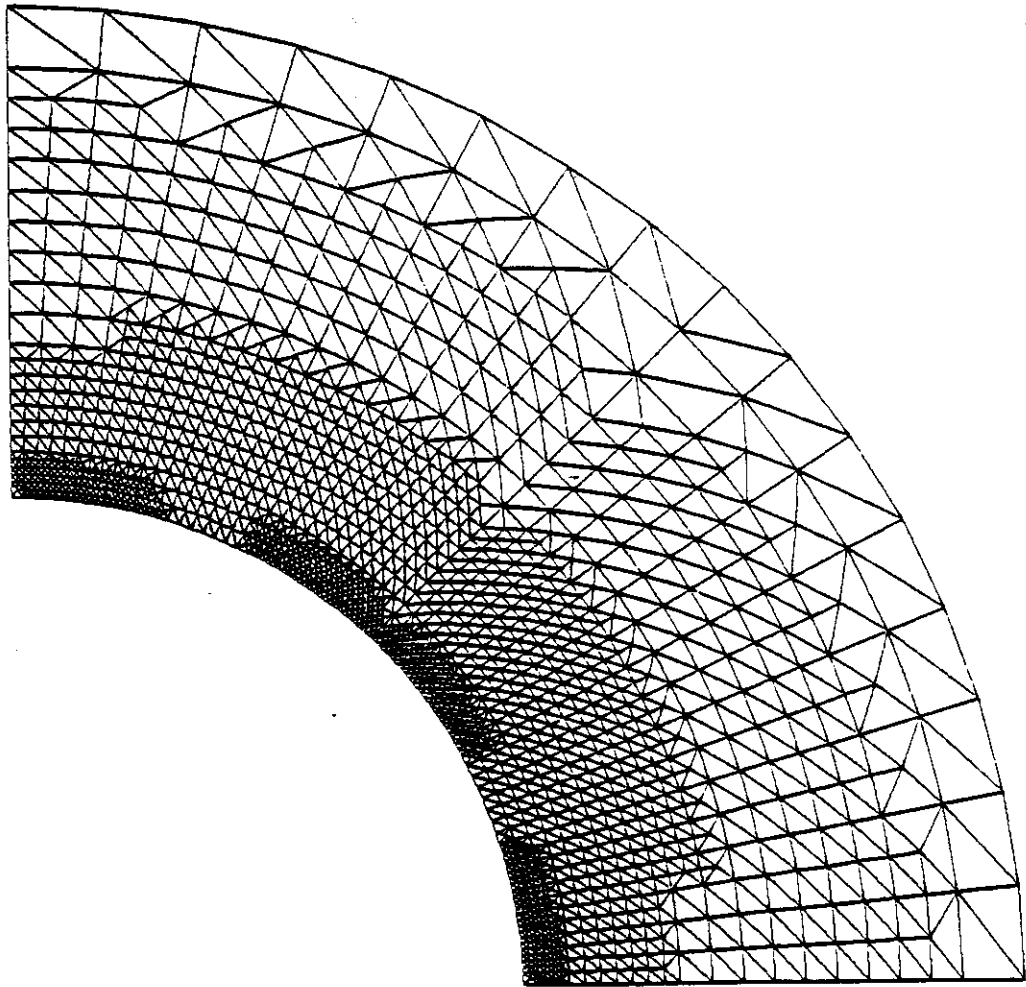


Figure 30: Example no. 2, mesh at iteration 7

TABLE 9

Example no. 2, Highest Error Stress Tensor Norms  
(Error Tolerance 1.5 ksi)

$X_1$	$X_2$	$\ \epsilon_{ij}\ $
.425	.904	1.299
.904	.425	1.299
.893	.447	1.295
.447	.893	1.295

#### 7.4 EXAMPLE NO. 3

The third example consists of the analysis of a thin circular disk under pinching load as shown in figure 32. The thickness of the plate is 0.1 inches and the material properties are:

Young modulus 30,000 ksi,

Poisson ratio 0.3

yield stress 50 ksi.

Since both the structure and the loading are doubly symmetric, the analysis has been run only for one quarter of the disk as shown in figure 33. The same figure also shows the patches used for modeling the structure. Two triangular patches are used. The small triangles represent the center point of each patch in the parametric space. The initial mesh is shown in figure 34. The input file is 20 lines long.

The error tolerance has been specified as 10% of the yield stress (5 ksi). The maximum number of iterations has been set to 9.

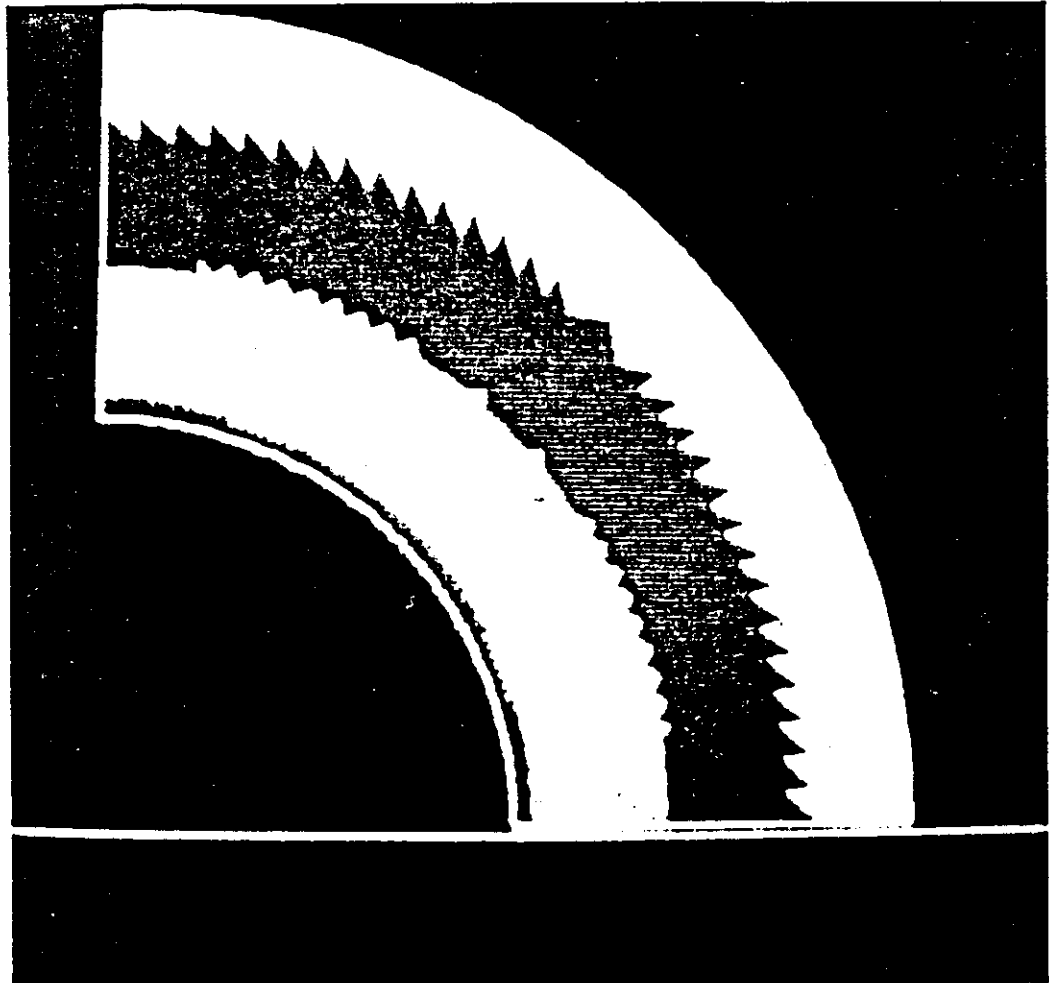


Figure 31: Example no. 2, color coded stress levels



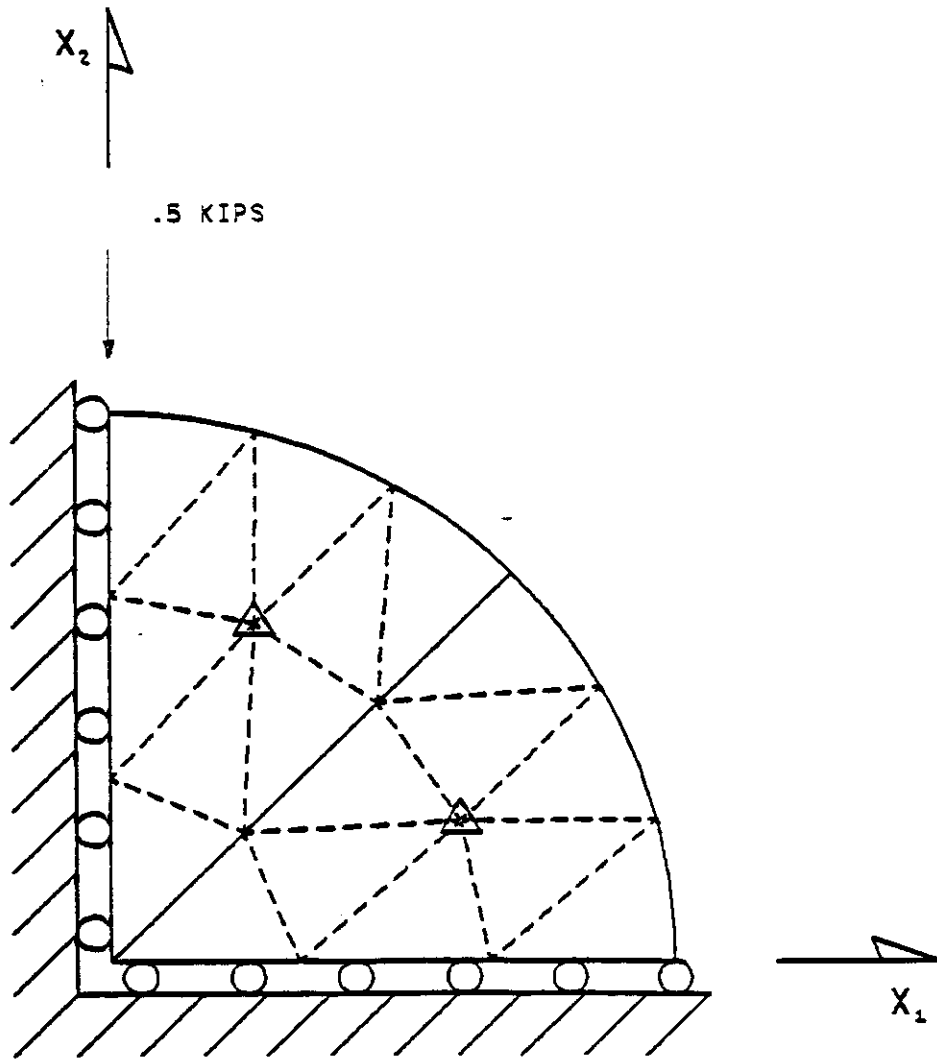


Figure 33: Example no. 3, input to the system

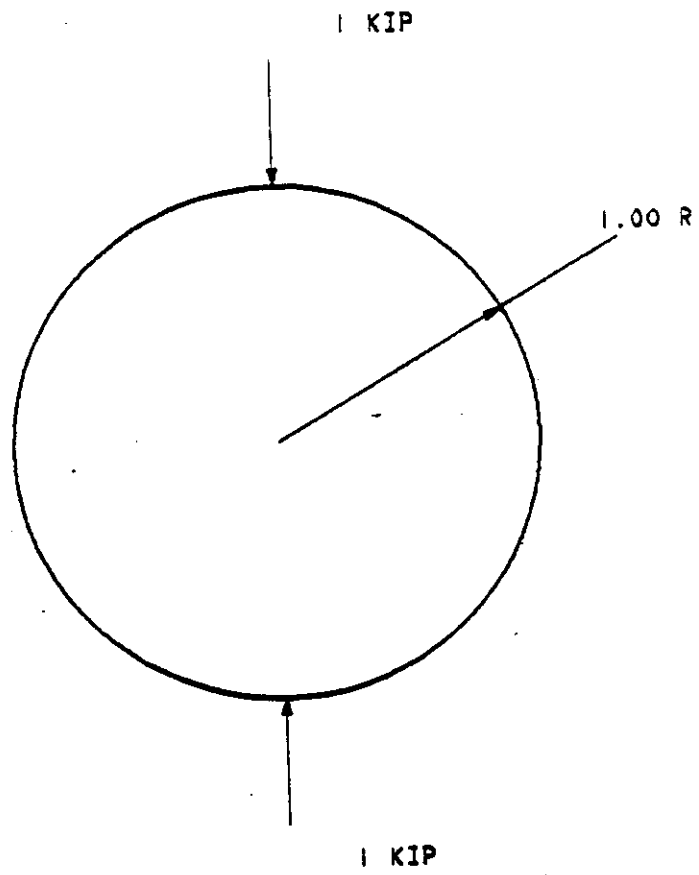


Figure 32: Example no. 3, description of the problem

As expected, convergence has not been reached due to the existence of a singularity. Also from iteration 5 on, the value of the largest norm of the error stress tensor for all triangles has kept increasing instead of decreasing. This can be explained by the fact that, as triangles become smaller and smaller, the error estimate becomes more and more precise and gives numbers that tend to be closer to the real error which is infinity.

The mesh at iterations 8 is shown in figure 35 and it consists of:

774 nodes,  
1504 degrees of freedom,  
1458 triangles.

In figure 36 the area where convergence has not been reached at iteration 8, is shown in yellow, the remaining area is shown in green.

The mesh at iterations 9 are shown in figures 37 and it consists of:

1578 nodes,  
3099 degrees of freedom,  
3032 triangles.

In figure 37 the dark area on the top of the quarter disk is due to the fact that the triangles size is smaller than the resolution of the plotter used to generate the picture. In figure 38 the area where convergence has not been reached at iteration 9, is shown in yellow, the remaining area is shown in green. Color coded stress levels at iteration 9, based on Von Mises criterion, are shown in figure 39. The lowest stress level is blue, the highest is red.

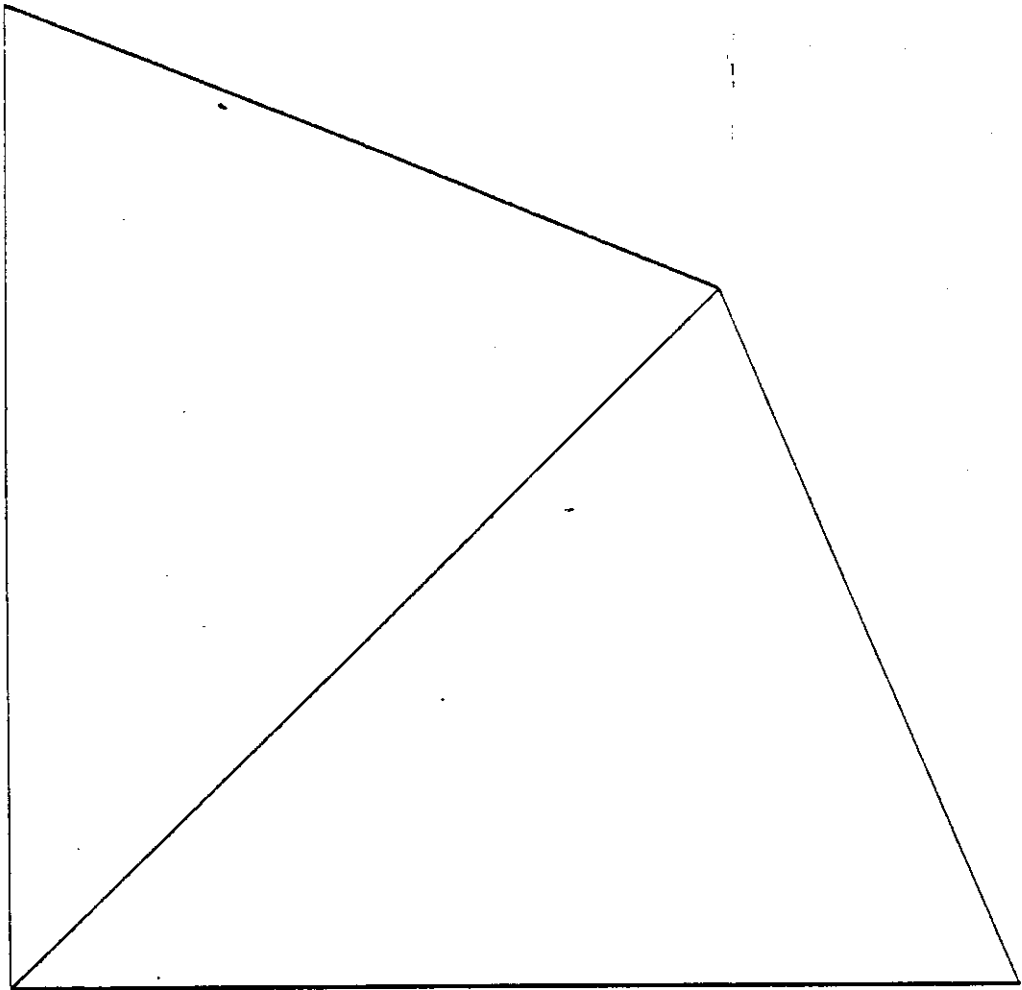


Figure 34: Example no. 3, initial mesh

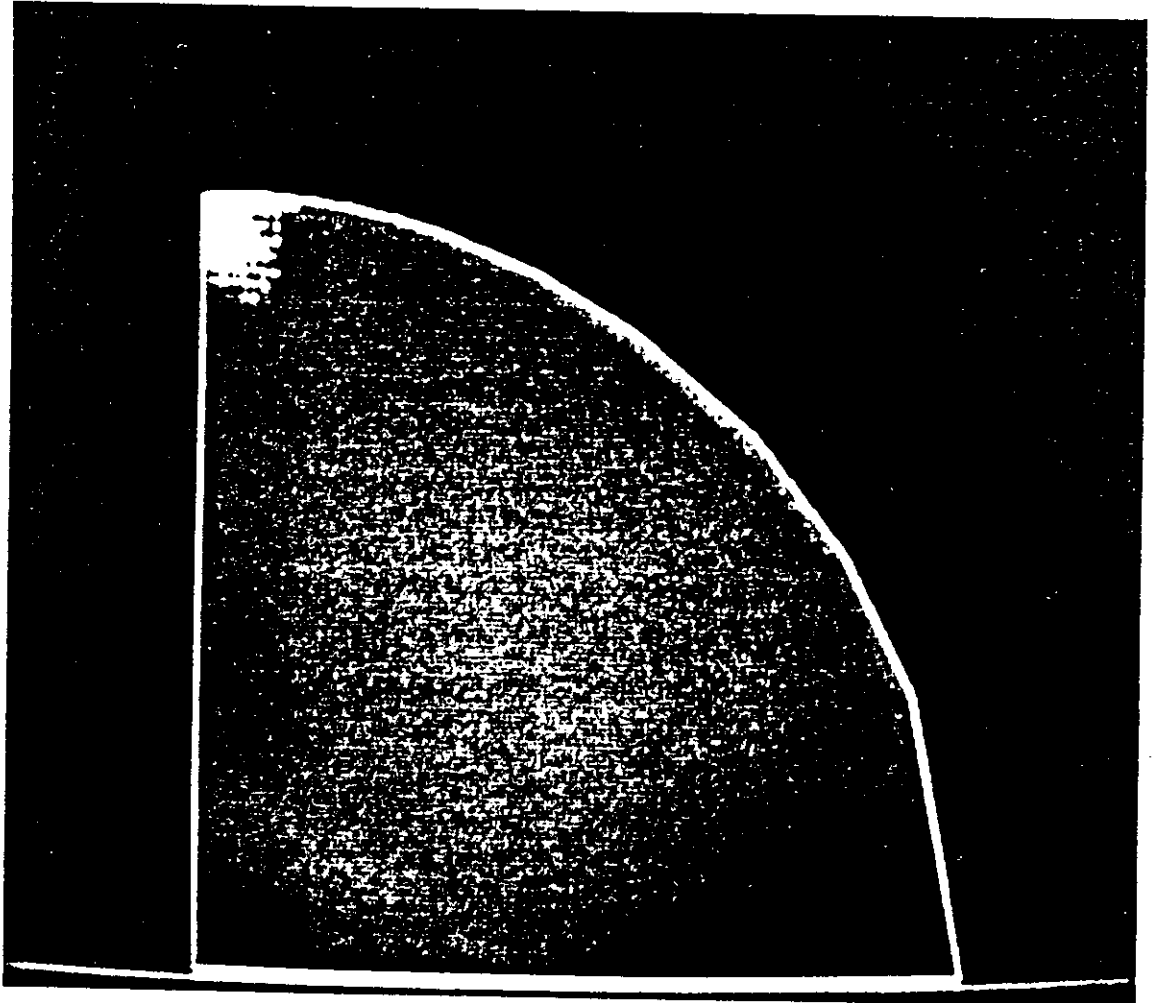


Figure 36: Example no. 3, non-converged area at iteration 8

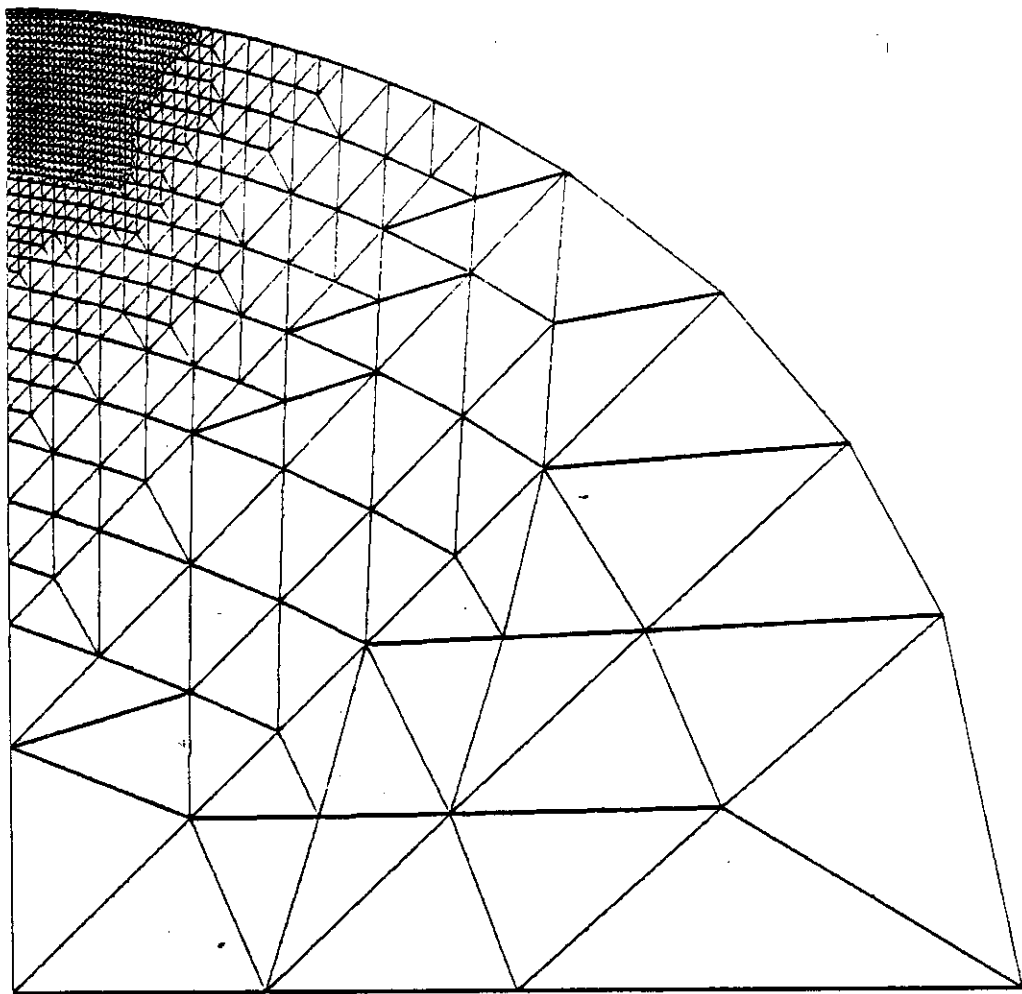


Figure 35: Example no. 3, mesh at iteration 8

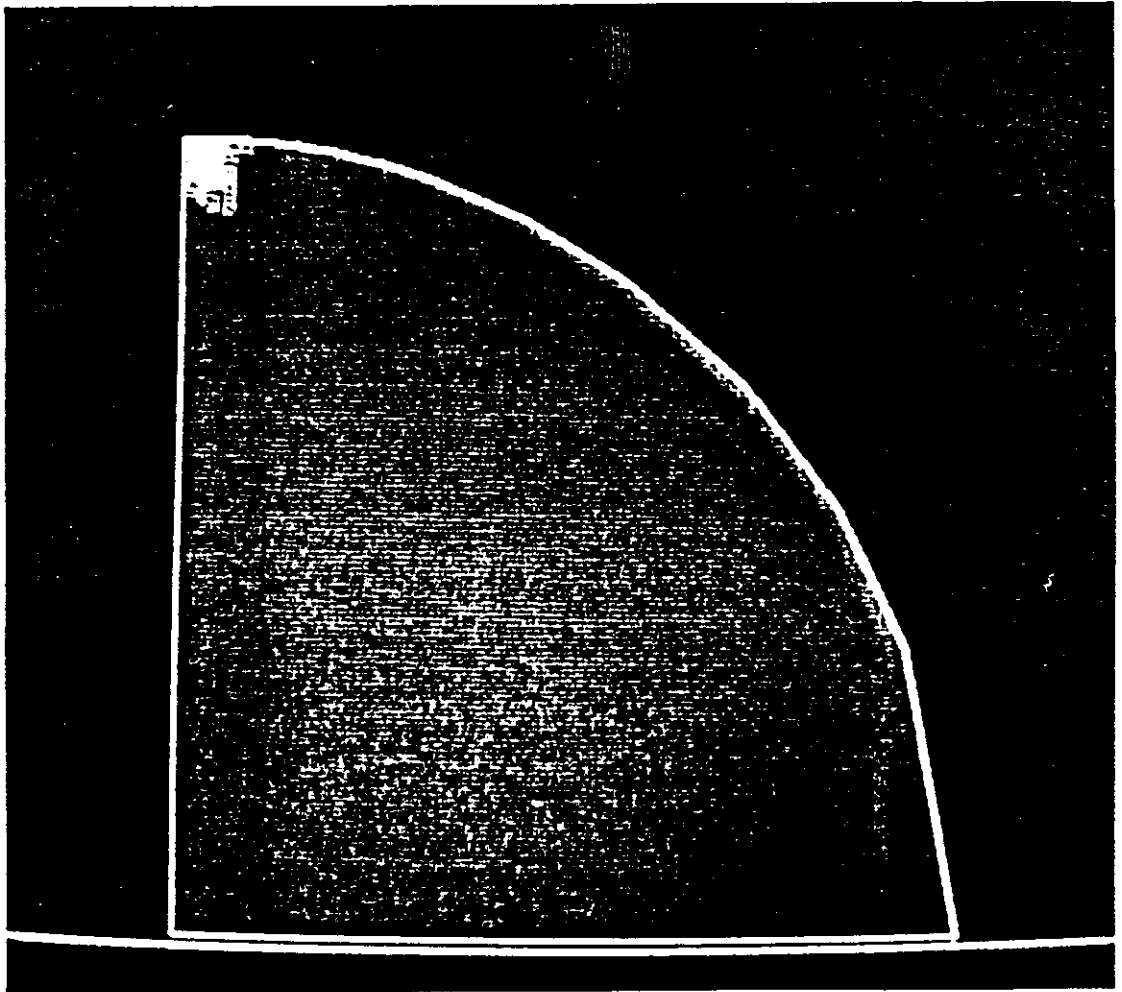


Figure 38: Example no. 3, non-converged area at iteration 9

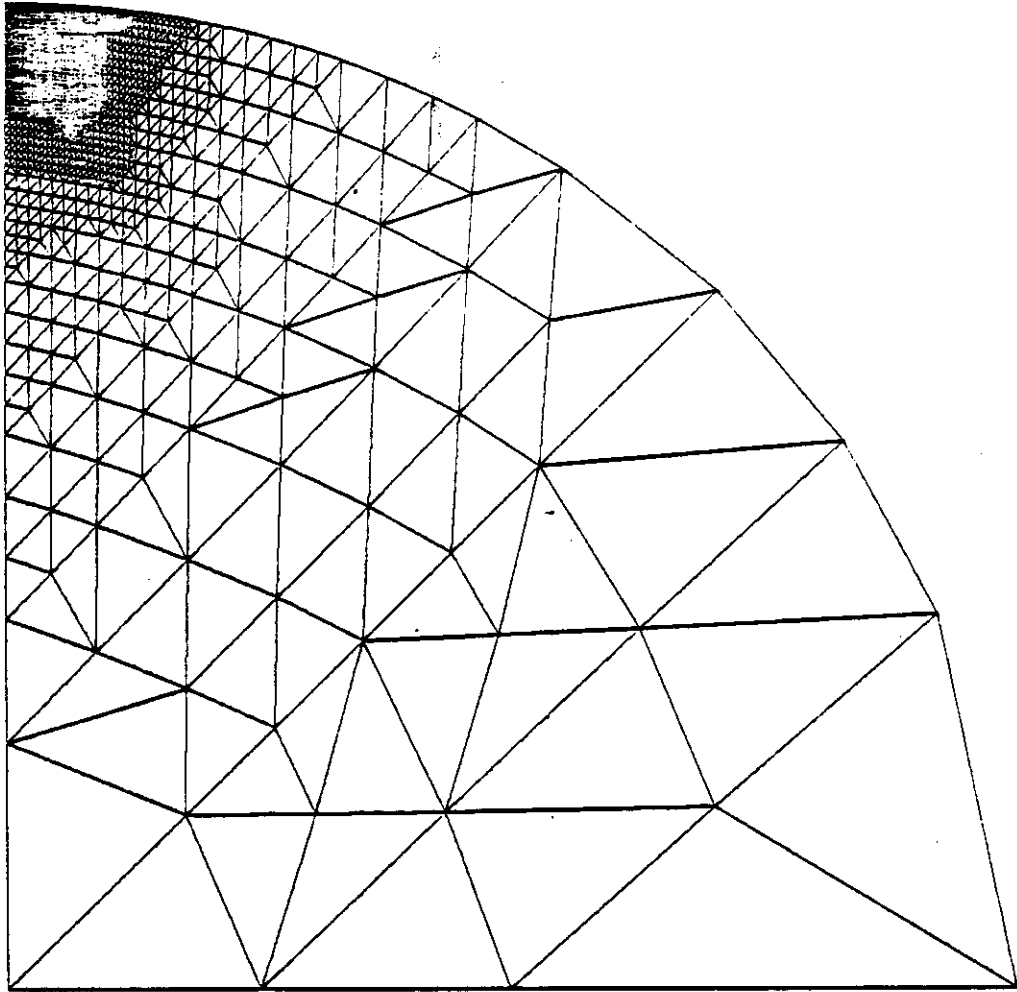


Figure 37: Example no. 3, mesh at iteration 9



Since the exact solution is available [ 2 ], the precision of the numerical results of iteration 8 and 9 has been checked for the triangles not marked for splitting. Before carrying out the actual calculations all triangles adjacent to triangles marked for splitting have also been marked and then the procedure has been repeated a second time. This is equivalent to step 2 and 3 of the splitting algorithm and is consistent with the reason why these steps have been introduced as discussed in the previous chapter.

In the mesh of the 8th iteration 962 triangles have not been marked for splitting. For all them the norm of the error stress tensor computed at each corner is less than the error tolerance.

In the mesh of the 9th iteration 2043 triangles have not been marked for splitting. At two of them at one corner each the error stress tensor norm is larger than the error tolerance (5 ksi). Both triangles lies in the area that was marked for splitting at iteration 8 and not marked for splitting at iteration 9. Their location thus is very close to the point of singularity.

In figure 40 the first of these two triangle is shown with the other three triangles that were generated when the triangles, that contains them all (parent triangle), has been split at iteration 8. The actual triangle is the top one an thus is an adjacent triangle. The corner at which the error stress tensor norm is larger than 5 ksi is marked with a small circle. The small triangular marker indicates the position of the centroid of the parent triangle.

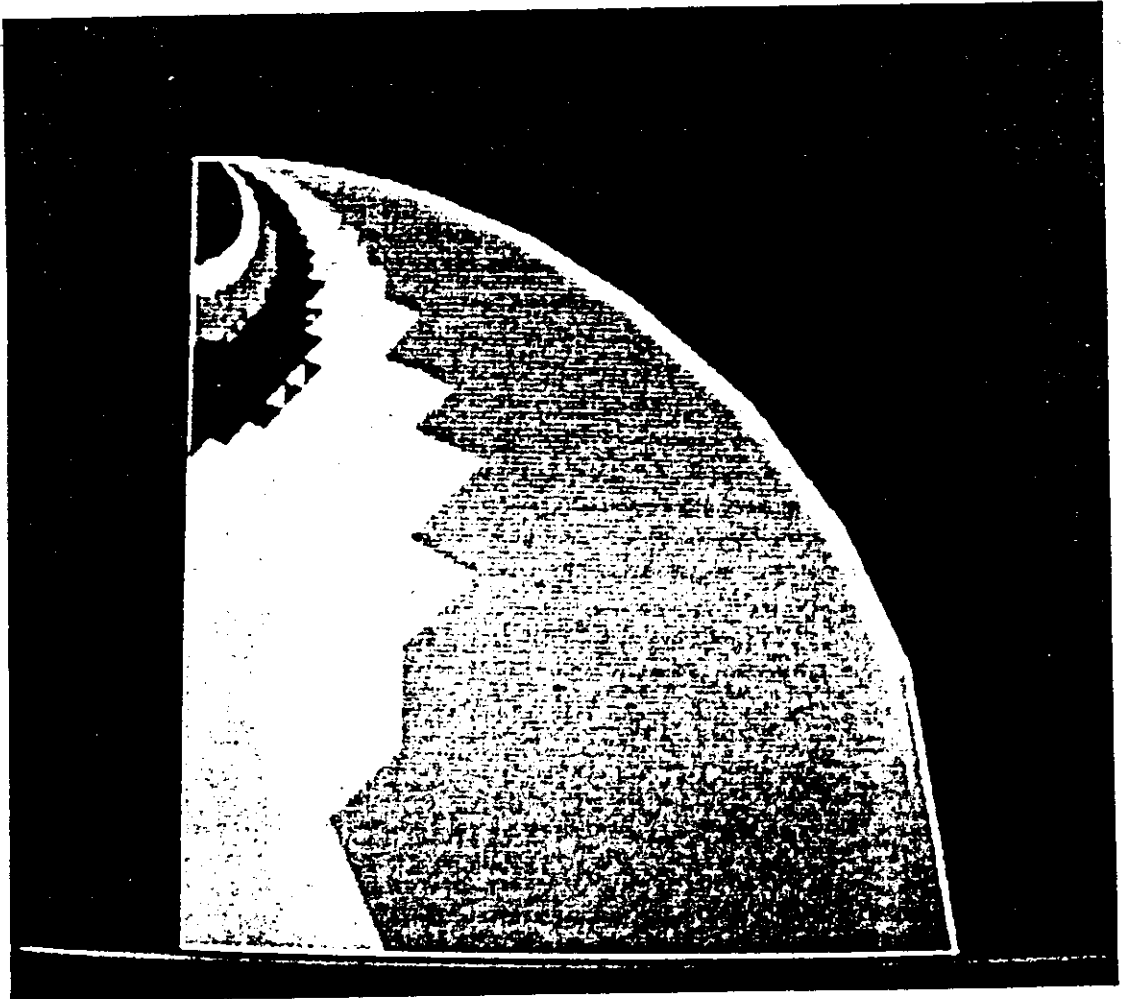


Figure 39: Example no. 3, color coded stress levels at iteration 9

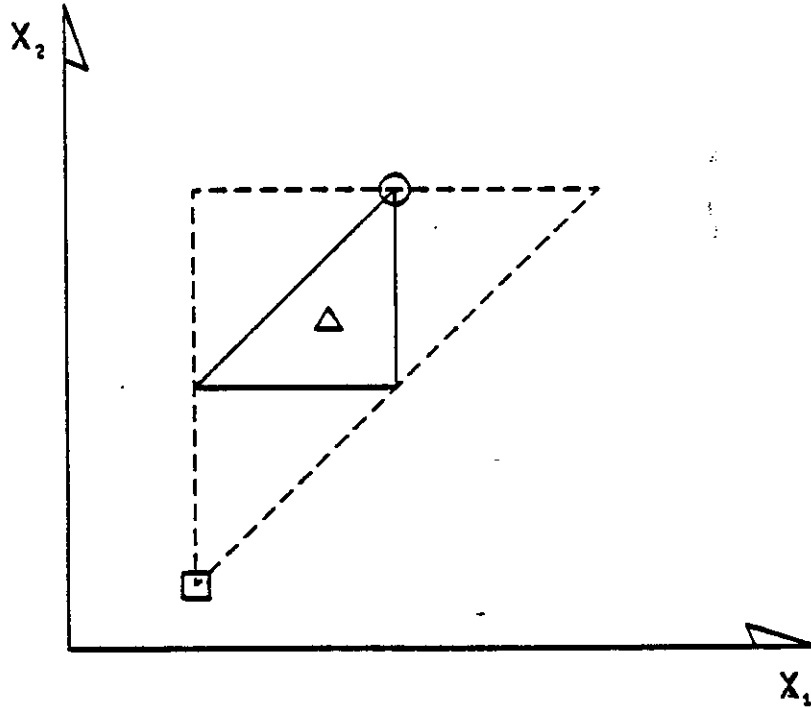


Figure 41: Triangle with error stress tensor norm larger than 5 ksi, case 2

In table 10 the exact, FEM, and error stresses at the first corner are listed. Also  $\delta_{ij}$  and its norm which is the error indicator is displayed. In the last line of the table the error in estimating each component of  $\varepsilon_{ij}$  and its norm is given. This error is given as a percentage of  $\|\varepsilon_{ij}\|$ . A plus sign means overestimation, a minus sign means underestimation. In table 11 the same information is listed for second corner.

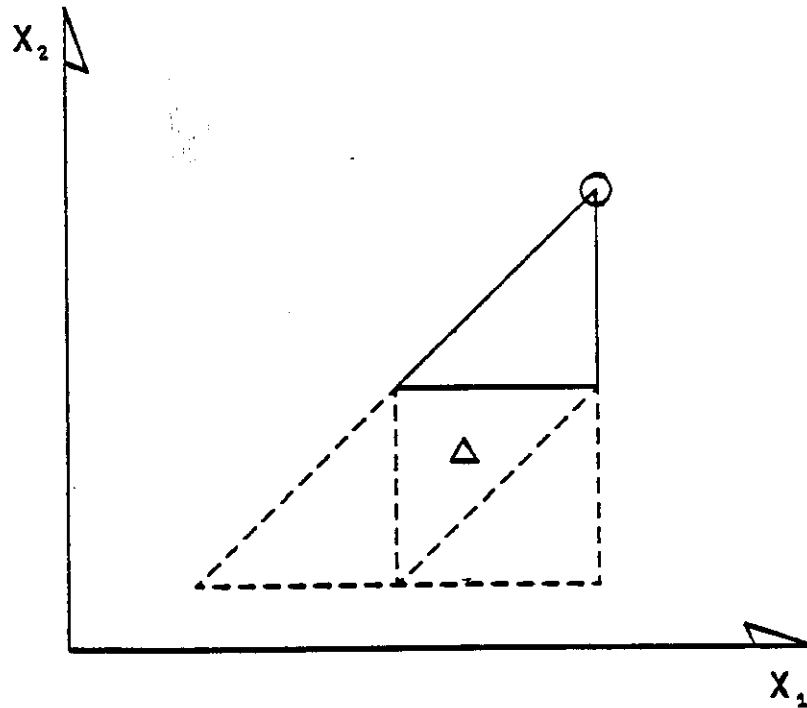


Figure 40: Triangle with error stress tensor norm larger than 5 ksi, case 1

In figure 41 the second triangle is shown in the same manner. It is a central triangle and the corner at which the error stress tensor norm is larger than 5 ksi is marked by a small circle.

The small triangular marker indicates the position of the centroid of the parent triangle. The little square marks the corner at which, according to the theory exposed in the previous chapter, the error stress tensor norm should have been detected as larger than 5 ksi.

In table 12 the exact stresses at the centroid of the parent triangle for the first case are listed. Also in the same table the FEM stresses and the error stresses at the same centroid are shown. In table 13 the same information is listed for the parent element of the second case.

TABLE 12

Stresses at the Centroid, Case 1  
(Error Tolerance 5 ksi)

---	i=1, j=1	i=2, j=2	i=1, j=2
$\sigma_{ij}^*$	2.868	-93.220	5.406
$\sigma_{ij}$	1.521	-93.210	4.058
$\epsilon_{ij}$	1.347	-.010	1.348

TABLE 13

Stresses at the Centroid, Case 2  
(Error Tolerance 5 ksi)

---	i=1, j=1	i=2, j=2	i=1, j=2
$\sigma_{ij}^*$	-2.114	-74.970	19.880
$\sigma_{ij}$	-4.015	-75.930	21.410
$\epsilon_{ij}$	1.901	.960	-1.530

A comparison of the numbers in tables 10 and 11 with tables 12 and 13 shows that the error at the centroid of the parent triangle is strongly linked to the error in estimating  $\epsilon_{ij}$ . For example in the

TABLE 10

Stresses at Corner, Case 1  
(Error Tolerance 5 ksi)

---	i=1, j=1	i=2, j=2	i=1, j=2	Norm
$\sigma_{ij}^*$	2.296	-99.701	9.388	---
$\sigma_{ij}$	2.175	-96.435	6.458	---
$\varepsilon_{ij}$	.121	3.266	2.930	5.277
$\delta_{ij}$	-.654	3.225	-2.401	4.728
Error Overest.	+8%	-1%	-10%	-10%

TABLE 11

Stresses at Corner, Case 2  
(Error Tolerance 5 ksi)

---	i=1, j=1	i=2, j=2	i=1, j=2	Norm
$\sigma_{ij}^*$	-3.157	-75.793	21.187	---
$\sigma_{ij}$	-1.463	-73.729	18.855	---
$\varepsilon_{ij}$	-1.694	-2.064	3.013	5.029
$\delta_{ij}$	-2.300	-1.440	2.710	4.696
Error Overest.	+14%	-12%	-6%	-7%

As can be seen the error stress tensor norm is underestimated by about 10% in the first case and 7% in the second case. Percentage of error underestimation for each component of  $\varepsilon_{ij}$  should be used only for qualitative comparisons since their values depends on the orientation of the reference axis.

TABLE 14

Taylor Series Expansion, Case 1

---	Constant	Linear	Residual
$\sigma_{11}$	2.868	-.386	-.186
$\sigma_{22}$	-93.220	-6.280	-.200
$\sigma_{12}$	5.406	3.484	.498

TABLE 15

Taylor Series Expansion, case 2

---	Constant	Linear	Residual
$\sigma_{11}$	-2.114	1.930	-.277
$\sigma_{22}$	-74.970	-1.800	.250
$\sigma_{12}$	19.880	-3.860	.240

exists between the actual error underestimation and the values of the residual terms.

first case,  $\epsilon_{22}$  at the centroid (.010 ksi, see table 12) is negligible compared with  $\epsilon_{22}$  at the corner (3.266 ksi, see table 10) and so is the underestimation of  $\epsilon_{22}$  which is 1% of  $\|\epsilon_{ij}\|$  (see table 10). Meanwhile, still in the first case,  $\epsilon_{12}$  at the centroid (1.347 ksi, see table 12) is of the same order of magnitude of  $\epsilon_{12}$  at the corner (2.930 ksi, see table 10) and the underestimation of  $\epsilon_{12}$  turns out to be 10% of  $\|\epsilon_{ij}\|$  (see table 10). This is a strong indication that the accuracy of the error estimate is strongly dependent on the fundamental assumption that at the centroid of any triangle the error of the stresses is negligible compared to the error at the corners.

The other fundamental assumption is that the exact solution for stresses can be assumed to be linear within each triangle. To see how correct this assumption is for the first case, the value of  $\sigma_{ij}^*$  have been computed at the corners marked by the small circle in figure 40 by taking the Taylor expansion at the centroid of the parent triangle. In table 14 the constant and linear terms as well as the residual of the Taylor expansion are listed for each stress component. The same procedure has been carried out for the second case. For consistency with the theory exposed in the previous chapter, the corner marked by the little square was use instead of the one marked by the small circle (see figure 41). The results are displayed in table 15

The residual terms indicates by how much  $\epsilon_{ij}$  could be underestimated due to the nonlinear behavior of  $\sigma_{ij}^*$ . In the worst case the value of the residual terms is about .5 ksi which is of the same order of magnitude of the error underestimation. However no coorelation



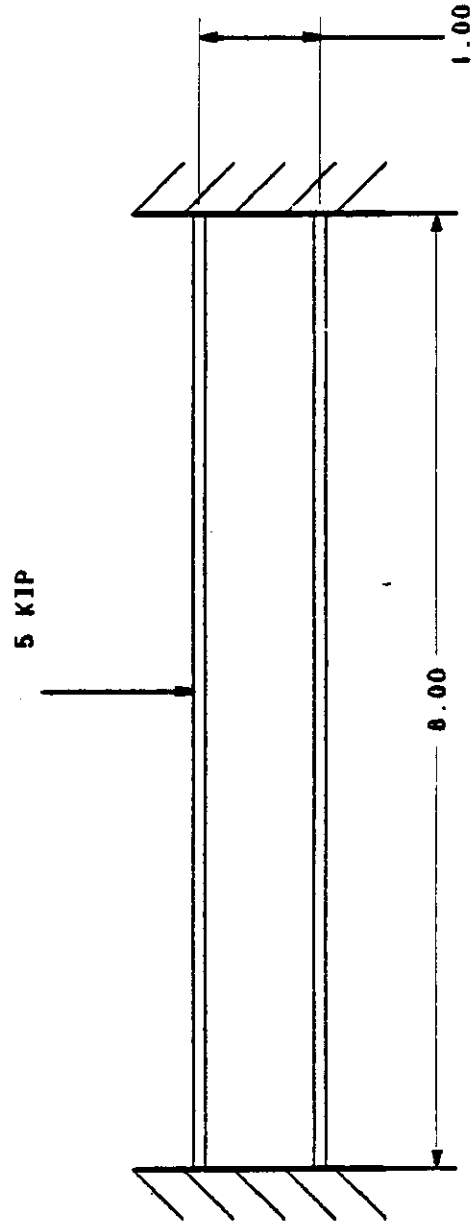


Figure 42: Example no. 4, description of the problem

## 7.5 EXAMPLE NO. 4

The fourth example consists of the analysis of a beam with flanges under a concentrated load applied in the center as shown in figure 42. The thickness of the web is 0.5 inches, The area of the flange is 0.5 square inches. The same material is used for both flanges and web. Its properties are:

Young modulus 10,000 ksi,

Poisson ratio 0.2

yield stress 10 ksi.

Since both the structure and the loading are symmetric the analysis has been run only for half of the beam as shown in figure 43. The same figure also shows the patches used for modeling the structure. The small triangles represent the center point of each patch in the parametric space. On the right edge the load has been evenly distributed along the web in order to avoid singularities. The left edge has been left free to move vertically in order to allow the web to expand freely, so that the solution is as close as possible to the beam theory solution. Consequently the reaction on the left edge has been modeled as a constant shear applied to the web. The pin on the lower left corner has been added to remove any rigid body motion. The input file is 35 lines long. The initial mesh is shown in figure 44.

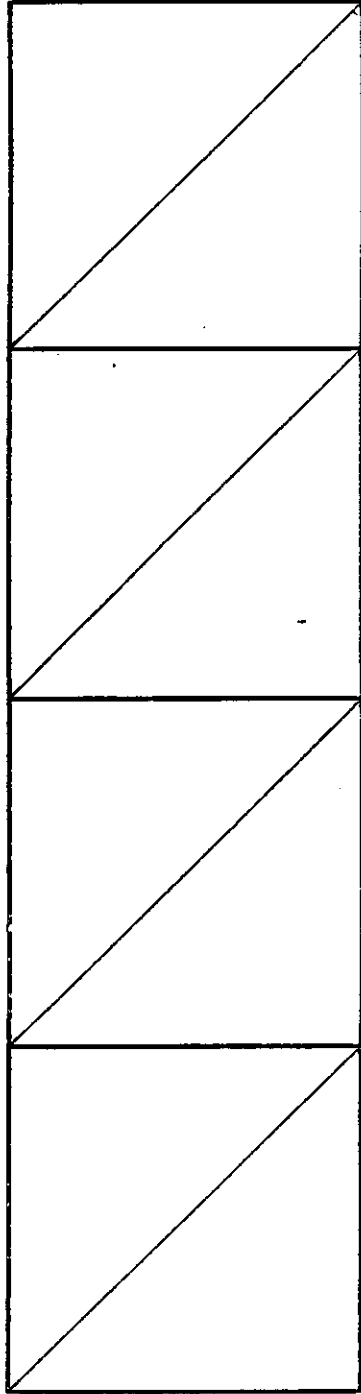


Figure 44: Example no. 4, mesh at iteration 1

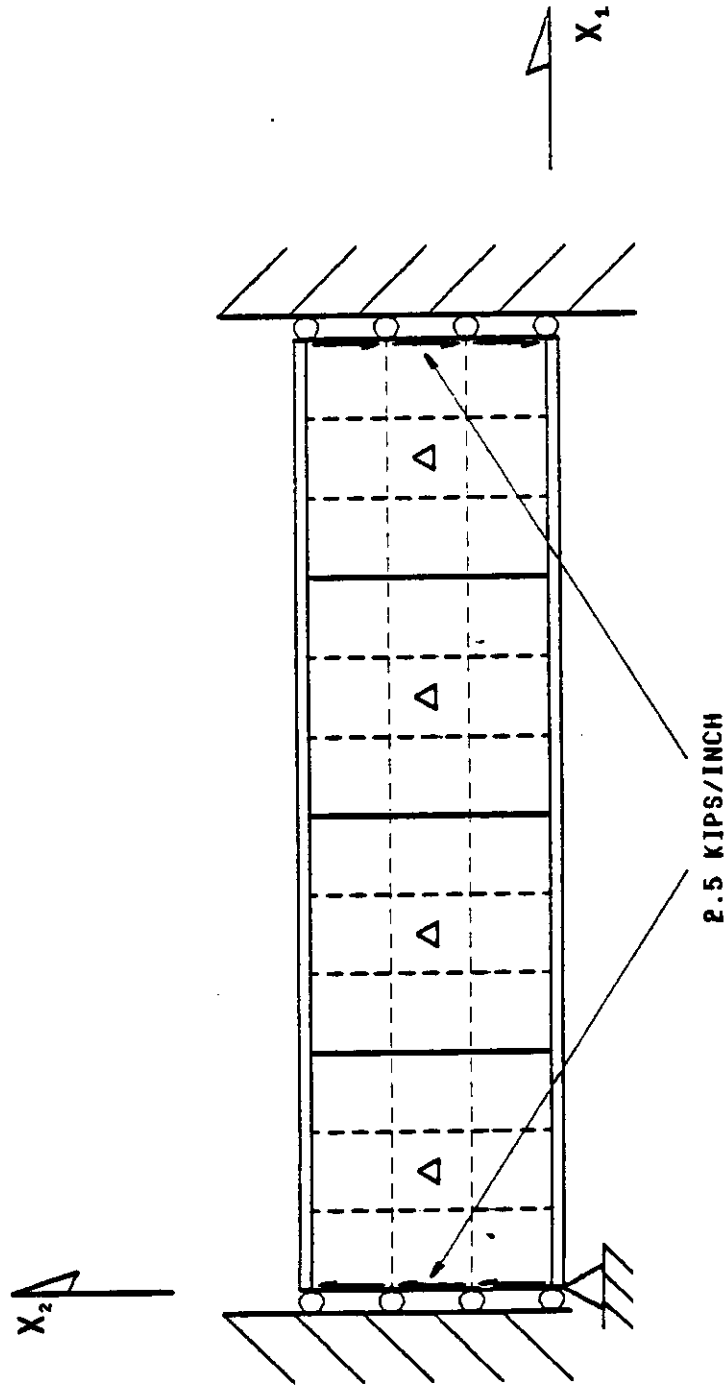


Figure 43: Example no. 4, input to the system

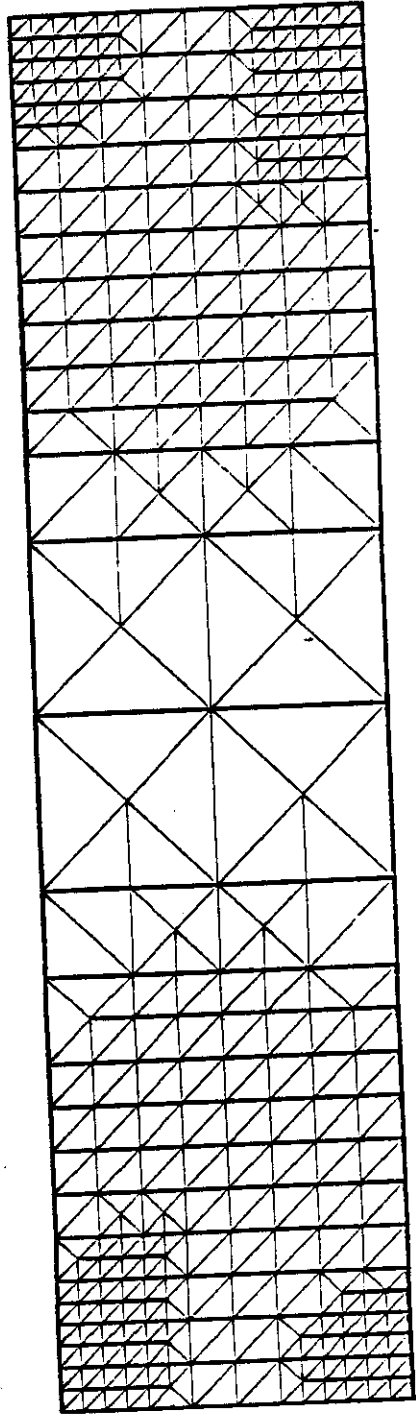


Figure 45: Example no. 4, mesh at iteration 5

The error tolerance has been specified as 25% of the yield stress (2.5 ksi) for both the flanges and web. Convergence has been reached in 5 iterations. The final mesh is shown in figure 45 and it consists of:

- 333 nodes,
- 645 degrees of freedom,
- 58 truss bars,
- 588 triangles.

Color coded stress levels in the flanges and web (based on Von Mises criterion) are respectively shown in figures 46 and 47. The lowest stress level is blue, the highest is red.

It is interesting to note that since the structure shown in figure 43 is symmetric and the load is antisymmetric the final mesh should be symmetric. The reason this does not happen is that, after the initial meshing, the model is not symmetric anymore.

To support this conclusion the example has been run a second time using the symmetric initial mesh shown in figure 48. Convergence was reached in 4 iterations, one less than in the first run since the triangle initially used in the corners are half in size of those used in the first run. The final mesh is shown in figure 49 and it is symmetric as expected. It consists of:

- 235 nodes,
- 439 degrees of freedom,
- 48 truss bars,
- 392 triangles.

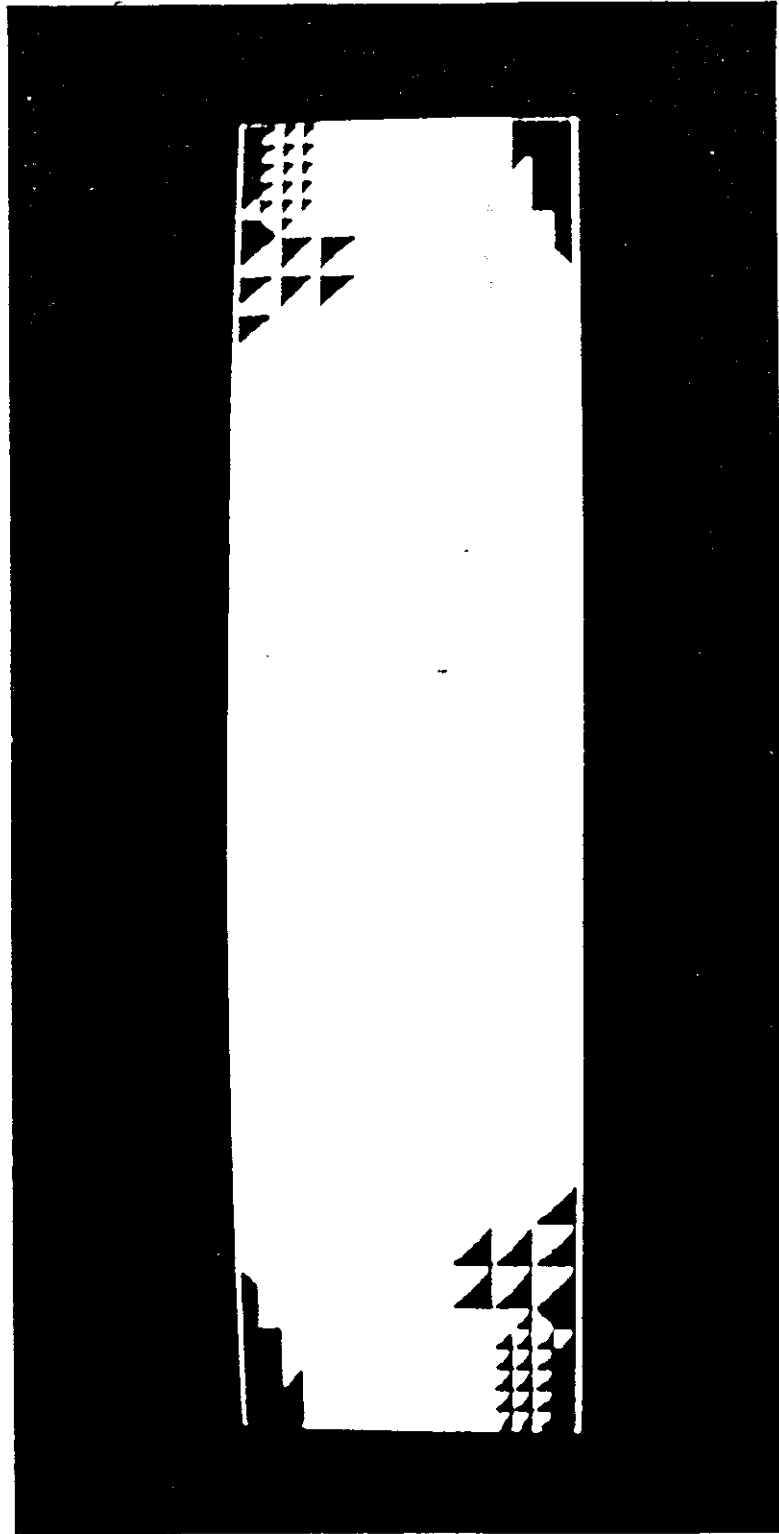


Figure 47: Example no. 4, color coded stress levels in the web

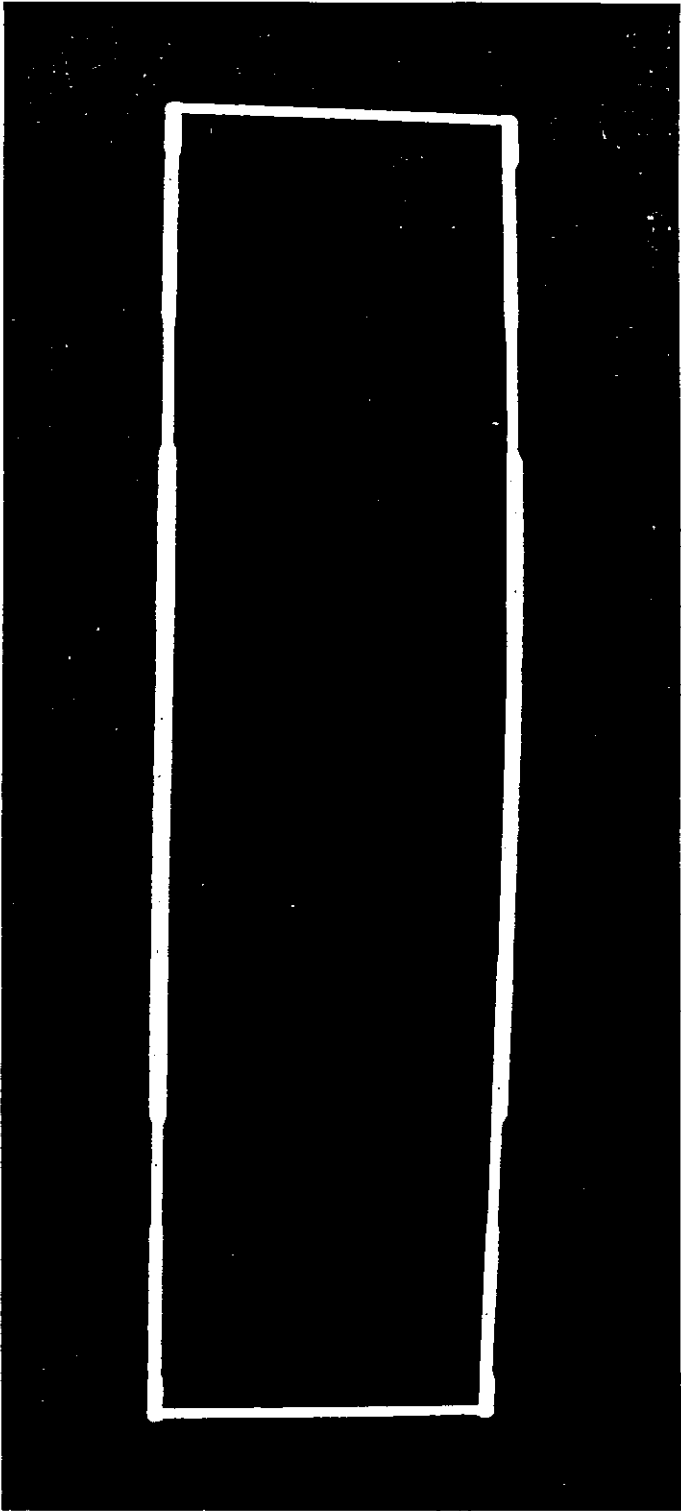


Figure 46: Example no. 4, color coded stress levels in the flanges



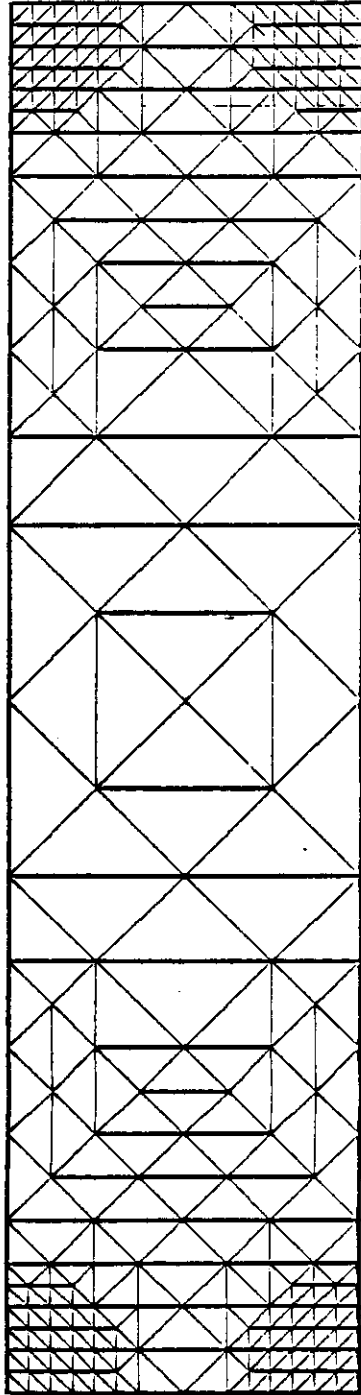


Figure 49: Example no. 3, final mesh second run

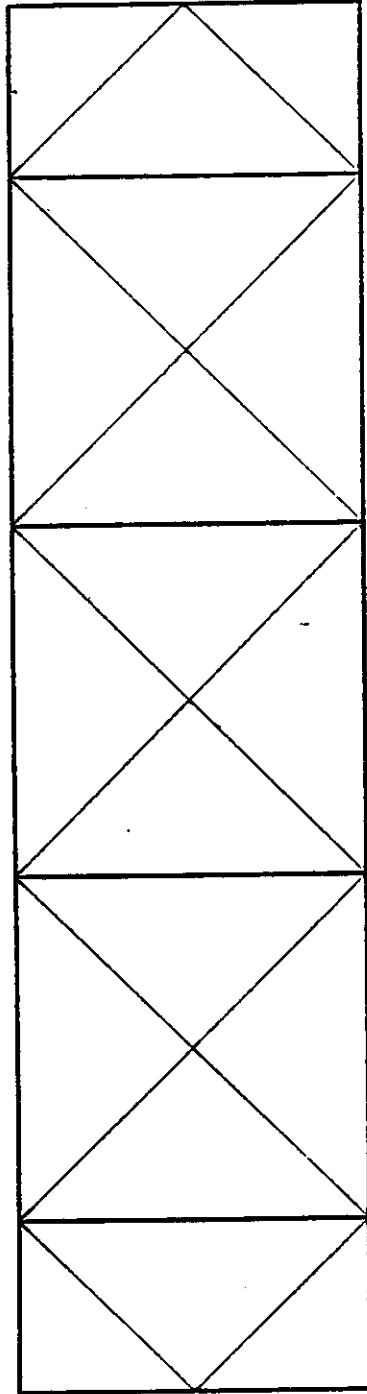


Figure 48: Example no. 4, initial mesh, second run

TABLE 17

Example no. 4, Highest Error of Axial Stress in Bars  
(Error Tolerance 2.5 ksi)

$X_1$	$X_2$	$\epsilon$
1.500	.000	1.125
2.500	1.000	1.125
2.500	.000	1.124
1.500	1.000	1.124

in the truss bars is much less than the error tolerance. This can be explained by the fact that all the bars were forced to be split by the triangles adjacent to them even though the error indicator was less than the error tolerance.

It should be noted that the beam theory solution is not the exact solution for this problem. For example the shear distribution at the web boundaries is constant for this example while it is parabolic in the beam theory solution. Still, since the error tolerance specified is not too small, the error due to the fact the the solution used for comparison is not exact, is negligible with respect to the error tolerance itself.

In fact the same example has been run for both initial meshes, with smaller error tolerances. As a result it is found that the smaller the error tolerance, the more numerous are the triangles with an error stress tensor norm larger than the error tolerance itself. On the other hand the error in the truss bars is always less than the

The results from the first and second run have been compared with the beam theory solution. The modality of the comparison is the same of the previous examples. In both cases, in all bars and triangles, the error is less than the error tolerance. This indicates again that the precision of the final solution is essentially independent of the initial mesh.

In table 16 the four highest error stress tensor norms found in corners of triangles are listed.

TABLE 16  
Example no. 4, Highest Error Stress Tensor Norms  
(Error Tolerance 2.5 ksi)

$X_1$	$X_2$	$\ e_{ij}\ $
1.250	.375	2.181
3.875	.625	2.181
4.000	.375	2.161
.000	.625	2.161

In the first two columns the points coordinates are given, in the third column the values of the norm are given. It can be seen that the error stress tensor norm is at all points is well below the error tolerance. In table 17 the four highest error stress found in bars' ends are listed.

In the first two columns the ends coordinates are given, in the third column the values of the error are given. It turns out that the error

## Chapter VIII

### EXTENSION OF THE PRESENT SYSTEM TO ANALYZE SHELL STRUCTURES

As stated in previous chapters, the system presented here has limited capabilities. It was also said that the generality of the approach used for this new system made it easy to expand its capabilities. In this chapter the extension of the present system to perform static analysis of shell structures will be discussed in some detail.

The extension of the present system to perform analysis of shell is straightforward. The shell could be described using the same patches extended to three dimensional space.

The elements used would be the constant strain triangle used in the present system coupled with any one of the triangular plate elements with 9 degrees of freedom available today.

Splitting of triangles and error computations would be done exactly in the same way as done on the present system. The only difference is that there would be two error computations, one for in-plane stresses and one for bending, each one with its own error tolerance. The error measurement for bending moments can be derived directly as it has been derived for stresses in 2-D, since bending moments are also 2-D tensors, as long as it is assumed that moments are constant all over the triangle. This assumption is not one hundred percent

error tolerance. This is consistent with the fact that the beam theory solution gives very accurate values for stresses in the flanges but not always in the webs as in this case.

Finally this example shows how simply the new system can handle structures with discontinuities as well as different types of structural elements.

## Chapter IX

### CONCLUSIONS

A new, design oriented approach to stress analysis has been developed. In this approach called "black box approach", FEM technology and a new self-adaptive mesh techniques have been combined to allow the structural designer to perform stress analysis without any knowledge of FEM. The key to this result has been the formulation of an algorithm which allows to determine with ease the error in the stress components for each element. This algorithm has been tailored to constant strain element.

A 2-D software system has been implemented to show how the black box approach works in practice. Examples shows that the system is behaving as expected. In fact the precision of the error estimate has been shown to be very accurate from an engineering point of view, which makes the system quite reliable.

The generality of the approach allows to expand the system with relative ease. The extension to static analysis of shell structure has been discussed in detail and it has been shown, that from a conceptual viewpoint, no additional work is necessary.

False convergence which is a potential problem has been discussed in some detail.

correct since in 9 DOF plate triangles there are always some modes shapes that represent linearly varying bending moments. However these modes shapes are incomplete and they do not contribute anything to the precision of the analysis.

From the computer implementation viewpoint the extension would require a significant amount of changes in the preprocessor and postprocessor. Relatively few changes would be required in the self-adaptive analysis module.



## Appendix A

### PRECISION OF ERROR ESTIMATE IN ONE DIMENSION

Let's consider the boundary problem in the form

$$u_{,xx} = f(x) \dots\dots\dots (A.1)$$

where  $x$  is such that  $0 \leq x \leq l$ . Boundary conditions can be any as long as they keep the problem self-adjoint. Let's consider now a point  $x_0$  such that  $0 \leq x \leq l$ . The solution for the first derivative around this point can be expressed as

$$u_{,x} = a_0 + a_n (\Delta x)^n \dots\dots\dots (A.2)$$

where  $a_0$  is the value of  $u_{,x}$  at  $x_0$  and  $a_n$  is the first non zero coefficient of the Taylor series expansion. Integrating once we get

$$u = c + a_0 (\Delta x) + a_n (\Delta x)^{n+1} / (n+1) \dots\dots\dots (A.3)$$

where the constant of integration  $c$  is the value of  $u$  at  $x_0$ .

Let's now consider two points at locations  $x_0 + d$  and  $x_0 + 2d$  such that  $(x_0 + 2d) \leq l$ . If FEM is used and the points at locations  $x_0$  and  $x_0 + 2d$  are contiguous nodal points, the solution at these points is exact because of superconvergence [ 3 ]. The first derivative between the two points is approximated by a constant function

$$s_0 = a_0 + 2^{n+1} a_n d^n / (n+1) \dots\dots\dots (A.4)$$

It is believed that this research proves convincingly that the black box approach is a viable way to perform stress analysis and that it can dramatically increase the reliability and usability of the Finite Element Method.

$$E_4 = ((n-1)2^n + 1)a_n d^n / (n+1) \dots \dots \dots (A.12)$$

By simple inspection is easy to notice that the point at which the true error is underestimated by the largest factor is at node  $x_0 + 2d$  in the second element, regardless the value of  $n$ . If we define  $r$  as the ratio between the true error and the error estimate we have

$$r = (n-1)n / (2^n - 1) \dots \dots \dots (A.13)$$

Equation A.13 gives the factor of how much the error is underestimated as a function of the polynomial content of the solution. If  $n=1$  then  $r$  becomes 1 and no underestimation takes place. Also it is important to notice that the error estimate of equations A.7 and A.8 is proportional to  $d$  and thus it is possible to identify the polynomial content of the solution by observing how the error estimate changes when a new nodal point is inserted in the middle of the first element and the all procedure is repeated again.

It should finally noted that this conclusion were reached using the Taylor series expansion. This requires that  $d$  itself has to be reasonably small. When  $d$  tends to zero equation A.13 becomes exact.

If the grid point at location  $x_0 + d$  is inserted, the approximate derivative between  $x_0$  and  $x_0 + d$  is approximated by

$$s_1 = a_0 + a_n d^n / (n+1) \dots \dots \dots (A.5)$$

and between  $x_0 + d$  and  $x_0 + 2d$  is approximated by

$$s_2 = a_0 + (2^{n+1} - 1)a_n d^n / (n+1) \dots \dots \dots (A.6)$$

The error estimate within the element connecting  $x_0 + d$  and  $x_0 + 2d$  is also

$$D_1 = |s_1 - s_0| = (2^n - 1)a_n d^n / (n+1) \dots \dots \dots (A.7)$$

The error estimate within the element connecting  $x_0$  and  $x_0 + d$  is

$$D_2 = |s_2 - s_0| = (2^n - 1)a_n d^n / (n+1) \dots \dots \dots (A.8)$$

It is possible now to compute the true error of the first derivative at the nodes of the two element. In the first element at node  $x_0$  the error is

$$E_1 = a_n d^n / (n+1) \dots \dots \dots (A.9)$$

In the first element at node  $x_0 + d$  the error is

$$E_2 = n a_n d^n / (n+1) \dots \dots \dots (A.10)$$

In the second element at node  $x_0 + d$  the error is

$$E_3 = |(2^n - n)a_n d^n / (n+1)| \dots \dots \dots (A.11)$$

In the second element at node  $x_0 + 2d$  the error is

13. M.S. Shephard, R.H. Gallagher and J.F. Abel, "Synthesis of Near-Optimum Finite Element Grids with Interactive Computer Graphics" International Journal for Numerical Methods in Engineering, Vol. 15, 1980, pp. 1021-1039.
14. M.S. Shephard, "Finite Element Grid Optimization-A Review", Finite Element Grid Optimization (Eds. M. S. Shephard and R. H. Gallagher), ASME Special Publ. PVP-38, 1979.
15. G.F. Carey and D.L. Humphrey "Residuals, Adaptive Refinement and Iterative Solution in Finite Element Computations", Finite Element Grid Optimization (Eds. M.S. Shephard and R.H. Gallagher), ASME Special Publ. PVP-38, 1979.
16. S.R. Gago, D.W. Kelly, O.C. Zienkiewicz "Adaptive Finite Element Schemes and A-Posteriori Error Analysis, an Evaluation of Alternatives." New and Future Developments in Commercial Finite Element Methods, (Ed J. Robinson), Third World Congress and Exhibiton on Finite Element Methods, pp. 512-528, 1981.
17. E.R.A. Olivera, "Optimization of Finite Element Solutions", Proc. 3rd Conf. on Matrix Methods in Structural Mechanics, Wright-Patterson Air Force Base, Ohio, October 1971.
18. D.W. Kelly, J.P. De, S.R. Gago, O.C. Zienkiewicz, L. Babuska "A Posteriori Error Analysis and Adaptive Processes in the Finite Element Method: Part I-Error Analysis." International Journal for Numerical Methods in Engineering, Vol. 19, 1983, pp. 1593-1619.
19. J.P. De, S.R. Gago, D.W. Kelly, O.C. Zienkiewicz, L. Babuska "A Posteriori Error Analysis and Adaptive Processes in the Finite Element Method: Part II-Adaptive Mesh Refinement." International Journal for Numerical Methods in Engineering, Vol. 19, 1983, pp. 1621-1656.

## REFERENCES

1. Y.C. Fung, Foundations of Solid Mechanics, Prentice Hall, Inc., New Jersey, 1965.
2. S.P. Timoshenko and J.N. Goodier, Theory of Elasticity, McGraw Hill Book Company, Inc., New York, 1951.
3. G. Strang and G.J. Fix, An Analysis of the Finite Element Method, Prentice Hall, Inc., New Jersey, 1973.
4. O.C. Zienkiewicz, The Finite Element Method, McGraw Hill Book Company, Inc., New York, 1977.
5. R.H. Gallagher, Finite Element Fundamentals, Prentice Hall, Inc., New Jersey, 1975.
6. K.J. Bathe and E.L. Wilson, Numerical Methods in Finite Element Analysis, Prentice Hall, Inc., New Jersey, 1976.
7. R.C.J. Howland, "On the Stresses in the Neighbourhood of a Circular Hole in a Strip Under Tension", Transactions, Royal Society of London, Vol. 229, 1930, page 49.
8. D.J. Turcke and G.M. McNeice, "Guidelines for Selecting Finite Element Grid Based on an Optimization Study", Computers and Structures, Vol. 4, 1974, pp. 499-519.
9. B.A. Szabo and A.K. Metha, "P-Convergent Finite Element Approximations in Fracture Mechanics", International Journal for Numerical Methods in Engineering, Vol. 12, 1978, pp. 551-560.
10. I. Babuska and W.C. Rheinbolt, "A-Posteriori Error Estimates for the Finite Element Method", International Journal for Numerical Methods in Engineering, Vol. 12, 1978, pp. 1597-1615.
11. A. Peano, R. Ricconi, A. Pasini and L. Sardella, "Adaptive Approximations in Finite Element Structural Analysis" Computers and Structures, Vol. 10, 1979, pp 333-342.
12. R.J. Melosh and P.V. Marcal, "An Energy Basis for Mesh Refinement of Structural Continua", International Journal for Numerical Methods in Engineering, Vol. 11, 1977, pp. 1083-1092.